Hindawi
Wireless Communications and Mobile Computing
Volume 2022, Article ID 5355854, 24 pages
https://doi.org/10.1155/2022/5355854

Research Article

Orbital Angular Momentum Wave Generation and Multiplexing: Experiments and Analysis Using Classical and Quantum Optics

Manisha Khulbe[1] **and Harish Parthasarathy**[2]

[1]*Dept. of Electronics and Communication Engineering, Netaji Subhash University of Technology, East Campus, (Formerly Ambedkar Institute of Advanced Communication Technologies and Research), N. Delhi, India*
[2]*Dept. of Electronics and Communication Engineering, Netaji Subhash University of Technology, Dwaraka, N. Delhi, India*

Correspondence should be addressed to Manisha Khulbe; manishakhulbe21@gmail.com

Received 26 May 2022; Revised 30 August 2022; Accepted 14 September 2022; Published 11 November 2022

Academic Editor: Yi Sun

Optical fiber communication is known as the backbone of communication today for voice, video, and data transmission. Recent advancements in optical technologies are leading us to many new forms of generation of orbital angular momentum (OAM) waves and its transmission technologies. Among them are hypergeometric waveform (HG), Bessel's waveforms, Laguerre Gaussian waveforms, and other forms of OAMs. This mode of communication is by the twisted form of electromagnetic wave which can accommodate a larger number of channels making communication simpler for wired and wireless communication. In this paper, various methods of OAM waveform generation are presented and are compared in details discussing the various needs in communication. OAM multiplexing is done by spatial division multiplexing (SDM) and wavelength division multiplexing (WDM). Methods of OAM communication, generation techniques, power analysis, and bit error analysis prove efficient transmission capability of OAM waves using low power consumption and low bit error rate in optical communication networks. OAM from fiber can be directly communicated to atmosphere which is found very useful for short distance wireless communication. Experimental validation is discussed for HG, Bessel's waveforms, and LG waveforms. Pure Optical Vertices (OV) are generated by VCSELs (vertical cavity surface emitting lasers) and transmitted by (MMF) multimode fibers. Various atmospheric effects and challenges are also elaborated in this paper. RSoft OptSim software is used for simulation.

1. Introduction

In traditional ways of communication generation of signals depend on frequency, time, and space, but these modes of communication are not sufficient to the present day need of high data transmission networks. In the field of optical communication, multi-input multioutput (MIMO) architecture employs a combination of OAM, spatial division multiplexing (SDM), and wavelength division multiplexing (WDM) [1–3]. The optical multiplexing system gives distinctive advantage over the other traditional multiplexing techniques. These multiplexing techniques include TDM, WDM, DWDM, OAM, SDM, and polarization division multiplexing (PDM) [1, 3, 4]. In both classical and quantum mechanics, angular momentum comprises SAM and OAM [1] in a combined form. OAM modes are mutually orthogonal, giving additional degree of freedom in multiplexing [1–3], increasing the data capacity of optical fibers [1, 2] in the terabit range. In WDM, one wavelength can carry multiple modes of OAM using a single multimode fiber [1, 3]. The vortex beam carries azimuthal component $\exp(jl\varnothing)$, where l is associated with OAM mode number an integer number. The screw type phase distribution is given by an OAM $\mp$ mh per photon [5, 6], where m is topological charge and h is plank's constant. The optical beams play an important role in optical communication and quantum computation [2, 7] especially used in mode division multiplexing and optical tweezers [8–10]. These optical vortices are created by spiral phase plates [6, 8, 9, 11] and computer generated fork holograms [11] and in optical domain by lasers. OAM multiplexing does not carry wavelength or polarization; OAM is used in addition to WDM

and PDM techniques in order to improve system capacity [2, 5, 8, 12, 13]. In demultiplexing the OAM waves, a spatial domain demultiplexer has photodetectors spatially arranged which are illuminated by each independent concentric ring; then separate individual SDM outputs are obtained. If we talk of quantum teleportation, a single photon is encoded in both spin and orbital angular momentum. The photon pairs are entangled in both degrees of freedom called hyper entanglement, which extends more degrees of freedom. These steps are towards more complex quantum system to control scalable quantum technologies [14]. In recent research photonic structures, metasurfaces [15] and dendritic cell clusters [16] are found useful for manipulation, transmission, and absorption of light. These metasurfaces give additional degrees of freedom to the polarization of light [17]. Some of the materials such as 2D Graphene, MoS2 molybdenum sulphide, and black phosphorous (BP) [18, 19] have properties of manipulating light in terms of polarization. These materials are proposed for OAM generation in photonic applications and also for wideband and wide-angle operation.

VCSELs have challenges as the modulation bandwidth is limited. It is of the order of several tens of GHz. So these VCSEL-based transmissions outperform electrical interconnect for long distances. VCSEL cell occupies a very small area of $\sim 10 \times 10\,\mu\text{m}^2$. One of the considerations is also the electronic optical routing of optical to electrical and electrical to optical conversion which is very costly in many ways. WDM is not spectrally efficient and consumes more power, so the solution lies in switching to the spatial dimension which is only viable optical routing scheme in optical interconnects. Spatial division multiplexing (SDM) and mode division multiplexing (MDM) use single wavelength. In OAM (m, l), m is the mode no. and l is the azimuthal no. in the cylindrical coordinate in MDM [20]. Dense wavelength-division multiplexing (DWDM) proves to give a multiplicative-factor 100 while transmitting data. SDM (space division multiplexing) also plays an important role in modern communication technology. It is accomplished by using the OAM technique [11] and overcame the shortcomings of the communication technologies such as TDM and DWDM in terms of channel capacity.

All channels are sharing the same physical space launched in different transverse modes in a physical channel. In the oceanic communication or seaside communication, OAM wave travels at the air water interface and faces underwater scattering/turbulence below the surface. This causes power loss and modal coupling in OAM-based optical links. Further investigation in underwater communication can be a challenge [21]. In atmosphere turbulence conditions, OAM communication leads to power fluctuation and link loss in the FSO system [21]. The solution is the BER performance in FSO which can be increased by mode diversity. In an underwater communication, OAM multiplexing techniques could potentially enhance the data rate capacity and it can lead to larger bandwidth [21].

OAM waves are twisted forms of light which are not used conventionally. This mode of communication is by photon flow. Different physical dimensions of photons include modulating, multiplexing, and multicasting data information. As the demand for more number of channel accommodation and internet traffic increases, this technology is giving more opportunities for multicasting and communication in turbulence [22–27] and is found to be the most suitable. OAM has attracted interest also in a nonlinear interaction of quanta-imaging and sensing [22].

In this paper, OAM generation, multiplexing, and demultiplexing of the optical signals are elaborated mathematically and experimentally. The photonic circuit in the RSoft OptSim module is used. OAM is not only used for wired but also for free space communication and wireless communication using planar-phased array antennas with PCB technology for radar imaging and MIMO application [28]. New techniques for radar imaging include quantum based measurement, which is far more precise than the classical methods. It can be carried out by OAM measurements only [2, 28, 29]. OAM is recognized as classical as well as quantum mechanics used in superresolution imaging. It has a linear momentum of electromagnetic wave at high frequency and has both spin and orbital angular momentum. Spin related to the polarization state and OAM is related to the helical phase front.

In sensing, we use nonclassical optical states such as phase, angular, and rotational variables and dispersive properties [28, 29]. Diffractive phase holograms, grating-based coupler waveguides, antenna arrays, spiral phase plate (SPP), holographic plate, and q plate are used for OAM generation.

In SAM, there are three possible polarization modes of EM beams, i.e., LHCP, RHCP, and linear polarization [2]. Plane waves in a free space have electric and magnetic field vectors which are orthogonal to each other and to their direction of propagation. In propagation of electromagnetic waves, the Poynting vector P is defined as $E \times H$ which determines the direction of propagation of power in an electromagnetic wave. Optical vortices have fruitful quantum properties. Photon is entangled in both space and polarization state. It is a classical entanglement [30]; high dimensional entanglement is used in channel coding to improve high capacity optical communication [30]. Optical vortices not only possess linear space application but also extensive uses in nonlinear communication with optical solitons [30]. Mode multiplexing increases tremendously in OAM wave in phased array structure antennas and in radar and MIMO applications [28]. An attractive feature is that OAM multiplexing can provide extremely high capacity with the existing modulation and multiplexing techniques. Conventional multiplexing schemes limit the communication capacity according to Shannon Cai et al. [31]. OAM, due to the spirally distributed phase and orthogonality and mode division multiplexing features, received widespread attention [29]. Nowadays, supervised and unsupervised learning techniques are being used to classify OAM states prorogating in a free space and a turbulent environment [29].

There is less coupling between adjacent modes with closet propagation mode [20]. This is the most important issue, as in conventional method signal processing is required to reduce mode coupling. Mode conversion efficiency is very high in OAM. Its components have zero static power consumption. Experimental results obtained almost zero power consumption in transreceivers. In the future, compact silicon-based OAM transmitting [31] devices will be used in integrated devices and demultiplexing devices [32]. Free-space OAM transmission link finds application in interlinks, while fiber-based OAM has application at the interrack level. So OAM finds application in

optical interconnects where extremely high capacity (density) is needed for sub mm confined spaces [33].

Silicon photonics with integrated OAM emitters convert waveguide modes into free space OAM modes [34]. Micro-sized spiral phase plates (SPPs) are fitted [35] in the aperture of VCSEL. OAMs are giving an unbounded number of possible states; hence, it is of great interest in optical communication, microscopy, sensing, and quantum optics. Because of low fabrication cost and high energy efficiency, this will become the future communication boon for society. Other than this, it also has high modulation bandwidth.

OAMs are achieved by an azimuthal varying phase achieved by bulk spatial light modulators (SLMs). It is an attractive device for a single photon device generation required in QKD Quantum Key distribution. OAM also contributes in optical trapping, quantum metrology, and remote detection. VCSEL aperture, each with its own integrated SPP, modulates the signal [26] incoming with data. OAM multiplexing, having a good modulation bandwidth, is giving several GHz of multiplexed bandwidth. Metasurfaces are also new techniques to be used for multiple OAM beam [36] generation.

The twisted form of an electromagnetic wave works on either spin momentum or angular momentum of light. OAM beams are orthogonal to each other, minimizing cross-talks between each other. Orthogonal beams can be made by Hermite–Gaussian beams without having an OAM pattern, but with the advantages of circular symmetry [37]. It can be used with already available commercial components. Moreover, these are also being used in free space communication. The advantages of using OAM is that almost zero power link can be established without much modification in the available systems. A single core can carry multiple OAM modes. Using VCSELs, the systems in transmitting and receiving are minimized, which leads to reduction of cost, size, and an increase of performance [26, 36, 37].

Earlier results with experiments have been presented for Terabit communication link using 16 QAM and QPSK signals [23–25, 37]. Experimentation shows multiplexing from 1550 nm to 1570 nm wavelengths. Though the experiment was done for only four wavelengths, it can be extended to more numbers of wavelengths. As a higher number of modes diverge more rapidly [37] than a Gaussian beam with lower order modes, it consumes less energy. Other than this, OAM multiplexing has grown so rapidly that we are using it in multiplying free space communication and underwater communication. Optical signal in underwater communication has higher data rates [31]. OAM modes are based on MIMO/SMM, resulting in four OAM multiplexed channels shown [23–25] for turbulent-free FSO link. In this experiment, each OAM mode carries a 100 Gbit/s quadrature phase-shift keying signal. The OAM/WDM-MIMO-based SDM and MDM [23] with a 1550 nm wavelength prove to give low bit error rate and turbulent-free wave propagation in FSO-optical links with QPSK input signals. Similarly, 4-level PAM [24] using OAM waves for 1600Gbps has been successfully implemented for FSO links. OAM with MIMO using PAM, QPSK, and QAM is coming with mitigating effects of atmospheric turbulence.

2. Mathematical Analysis of OAM Wave Generation

From a classical theory of electromagnetic wave generation, a three-dimensional Helmholtz equation is the temporal transform of the 3D wave equation. It describes the propagation of electromagnetic waves $\Psi(t, r)$ in a medium having spatially dependent refractive index $n(r)$.

$$\left[\nabla^2 - \frac{n^2(r)}{c^2}\frac{\partial^2}{\partial t^2}\right]\Psi(t, r) = 0. \tag{1}$$

On Fourier Transforms of this equation w.r.t to t, it is defined by

$$\widehat{\psi}\left(\frac{\omega}{c}, r\right) = \int_{IR} \psi(t, r) e^{-j\omega t} d\omega. \tag{2}$$

Or equivalently,

$$\psi(t, r) = \frac{1}{2\pi}\int_{IR} \psi\left(\frac{\omega}{c}, r\right) e^{-j\omega t} d\omega. \tag{3}$$

In terms of propagation constant k [38], the equation can be written as

$$\left(\nabla^2 + k^2 n^2(r)\right)\widehat{\psi}(t, r) = 0. \tag{4}$$

In a spherical polar coordinate [33] Appendix A.1,

$$\left(\frac{1}{r^2}\frac{\partial}{\partial r} r^2 \frac{\partial}{\partial r} - \frac{L^2}{r^2} + k^2 n^2(r)\right)\widehat{\psi}(t, r) = 0, \tag{5}$$

where $L^2 = L_x{}^2 + L_y{}^2 + L_z{}^2$ is the angular momentum square operator for three-dimensional components (x, y, and z) used in quantum mechanics. $\vec{L} = ' - i\vec{r}x\vec{\nabla}$, where r is position.

$$\begin{aligned}
Lx &= -i\left(Y\frac{\partial}{\partial t} - Z\frac{\partial}{\partial y}\right),\\
L_Y &= -i\left(X\frac{\partial}{\partial t} - Z\frac{\partial}{\partial z}\right),\\
L_Z &= -i\left(Y\frac{\partial}{\partial t} - X\frac{\partial}{\partial x}\right),\\
L^2 = L_x{}^2 + L_y{}^2 + L_z{}^2 &= -\left(\frac{1}{\sin\theta}\frac{\partial}{\partial\theta}\sin\theta\frac{\partial}{\partial\theta} + \frac{1}{\sin^2\theta}\frac{\partial^2}{\partial p^2}\right).
\end{aligned} \tag{6}$$

It gives solution

$$|l_1 m> \Delta Y_{lm}(\theta, \varnothing). \tag{7}$$

Thus adopting the separation of variables,

$$\widehat{\psi}(k, r) = R_k(r) Y_{lm}(\theta, \phi), \tag{8}$$

where $R < |r|, l, m$ are the modes in azimuth and spin number of the atoms (Appendix A.2 and A.3).

l is an integer. The radial equation can be defined in terms of refractive index n and propagation constant k using separation of variables [38] by

$$R_k{}''(r) + \frac{2}{r}R_k{}'(r) + \left(\frac{-l(l+1)}{r^2} + k^2n^2(r)\right)R_k(r),$$
$$r^2R_k{}''(r) + 2rR_k'(r) + \left(k^2r^2n^2(r)' - l(l+1)\right)R_k(r) = 0. \tag{9}$$

For different values of k, the radial component $R_k(r)$ of the em field are mutually orthogonal:

$$r^2R''_{k_1}(r) + 2rR'_{k_1}(r) + \left(k_1{}^2r^2n^2(r)' - l(l+1)\right)R_{k_1}(r) = 0,$$
$$r^2R''_{k_2}(r) + 2rR'_{k_2}(r) + \left(k_2{}^2r^2n^2(r) - l(l+1)\right)R_{k_2}(r) = 0,$$
$$r^2\left(R''_{k_1}R_{k_2} - R''_{k_2}R_{k_1}\right) + 2r\left(R'_{k_1}R_{k_2} - R'_{k_2}R_{k_1}\right) + \left(k_1{}^2 - k_2{}^2\right)r^2n^2(r)R_{k_1}(r)R_{k_2}(r) = 0,$$
$$L^2Y(\theta,\phi) = \lambda\hbar^2L. \tag{10}$$

λ^2 is an eigenvalue of the operator L^2 given by (Appendix A.2 and A.3)

$$\lambda = l(l+1)\ [l = 0, 1, 2, 3, \cdots],$$
$$L^2|l_1m> = l(l+1)|l_1m>. \tag{11}$$

2.1. Orthogonality of OAM Waves. Continuing from earlier equations,

$$\frac{d}{dr}\left(r^2\left(R'_{k_1}R_{k_2} - R'_{k_2}R_{k_1}\right) + \left(k_1{}^2 - k_2{}^2\right)r^2n^2(r)R_{k_2}R_{k_1} = 0.\right. \tag{12}$$

So again that $R_{k_j}(r) = O(1/r)$. We go on integrating the above equation.

$$\left(k_1{}^2 - k_2{}^2\right)\int_0^\infty r^2n^2(r)R_{k_1}(r)R_{k_2}(r)\mathrm{d}r = 0,$$
$$\text{So}\int_0^\infty r^2n^2(r)R_{k_1}(r)R_{k_2}(r)\mathrm{d}r = 0\ k_1{}^2 \neq k_2{}^2. \tag{13}$$

For cylindrical coordinates to solve the Helmholtz equation in a refractive index fluid $n(\rho)$, in terms of radial distance$\rho, n(\rho)=\sqrt{x^2} + y^2$. Then, the equation is

$$\left(\frac{1}{\rho}\frac{\partial}{\partial\rho}\rho\frac{\partial}{\partial\rho} + \frac{1}{\rho^2}\frac{\partial^2}{\partial\varnothing^2} + \frac{\partial^2}{\partial z^2} + k^2n^2(\rho)\right)\widehat{\psi}(k,\rho,\varnothing,z) = 0. \tag{14}$$

In the equation, $\psi(\rho)\propto\exp\left((-\rho^2/\omega_0{}^2)\right)$ is the complex electric field. ρ is the field distance from the center axis of the Gaussian beam. ω_0 is the center of the width of the wave, and l is the topological charge of OAM. $\varnothing$ is the azimuthal angle [39]. Such OAM beams have a helical phase structure with its wave front resembling l fold corkscrew pattern [9]. Such wave has an angular momentum along the beam axis given by exp $(i.l.\varnothing)$ around the beam, and hence, it has a spin and angular momentum both derived from Maxwell's equations.

Wave equation in terms of propagation constant β, ρ, $\varnothing, z$

$$\widehat{\psi}(k,\rho,\varnothing,z) = R_k(\rho,\varnothing)e^{-j\beta z},$$
$$\left(\frac{\partial^2}{\partial\rho^2} + \frac{1}{\rho}\frac{\partial}{\partial\rho} + \frac{1}{\rho^2}\frac{\partial^2}{\partial\varnothing^2} - \beta^2 + k^2n^2(\rho)\right)R_k(\rho,\varnothing) = 0, \tag{15}$$

where β denotes the propagation constant denoting the z direction. Information-carrying OAM beams [6] are given by $\Psi(\rho,\varnothing) = \Psi(\rho)\exp(i.l.\varnothing)$ by attaching a spiral phase mask (exp $(il\varnothing)$) to the Gaussian beam [10]. The encoding data can be described as $\psi(\rho,\varnothing,t) = \psi(\rho).\psi(t).\exp(i.l.\varnothing)$ where $\psi(t)$ is the data input. $k = 2\pi/\lambda$ is the free space wave number. The radial equation has solutions for β values at a given wavelength. These solutions will represent the guided modes [6, 12] of the fiber. We can find all guided modes by starting with $l = 0$ [6, 8, 9, 12]. These optical electromagnetic field modes are produced in the fiber by VSCEL lasers [12].

Further separating the variables,

$$R_k(\rho,\varnothing) = R_k(\rho)e^{i\omega\varnothing},$$
$$\left(\frac{\partial^2}{\partial\rho^2} + \frac{1}{\rho}\frac{\partial}{\partial\rho} + \frac{m^2}{\rho^2} - \beta^2 + k^2n^2(\rho)\right)R_k(\rho,\varnothing) = 0,$$
$$\text{Or}\ \rho^2R''_k(\rho) + \rho R'_k(\rho) + \left(\left(k^2 - \beta^2\right)\rho^2 - m^2\right)R_k(\rho) = 0. \tag{16}$$

From the equations [17, 18], L^2 commutes with$L$and two operators can be jointly diagonalized [38, 39] using the spherical harmonics.

The m field solution given by

$$R_k(\rho) = C_1(k)J_m\left(\sqrt{k^2 - \beta^2}\,\rho\right) + C_2(k)Y_m\left(\sqrt{k^2 - \beta^2}\,\rho\right), \tag{17}$$

where J_m, Y_m are, respectively, the Bessel and modified Bessel function of order m. If boundary conditions are imposed on $R_k(\rho)$ as for example, the waves propagate within an $a < \rho < b$ the optical fiber $R_k(a) = R_k(b)$ implying

$$\text{Det}\begin{pmatrix} J_m\left(a\sqrt{k^2 - \beta^2}\right) & Y_m\left(a\sqrt{k^2 - \beta^2}\right) \\ J_m\left(b\sqrt{k^2 - \beta^2}\right) & Y_m\left(b\sqrt{k^2 - \beta^2}\right) \end{pmatrix} = 0. \tag{18}$$

Implying that $\sqrt{k^2-\beta^2}$ can assume only discrete values, say

$$\sqrt{k^2-\beta^2}=h_n,\ n=1,2,\cdots,\ \text{or}\ \beta_n=\beta^2=\left(k^2-h_n{}^2\right)^{(1/2)},\ n=1,2\cdots[40]. \tag{19}$$

In quantum mechanical language, we can write [38]

$$R_k(\rho)=R_{k,m}(\rho)=\epsilon\mathscr{L}\{J_m(h_n\rho)Y_m(h_n\rho)\}, \tag{20}$$

with the total wave field given by

$$\begin{aligned} &R_k(\rho)e^{-i\beta z}e^{im\varnothing},\\ &=R_{k,m}(\rho)e^{-i\beta(k)z}e^{im\varnothing},\\ &\equiv|m,n>_k. \end{aligned} \tag{21}$$

So that the general solution at frequency $\omega=kc$ is given by the superposition [38].

$$\sum_{m,n}C_k(m,n)|m,n>_k. \tag{22}$$

Or in the time domain, by

$$\frac{c}{2\pi}\int\sum_{m,n}\sum_{m,n}C_k(m,n)|m,n>_k\quad e^{ik_c t}dk=\Psi(t,\rho,\phi,t). \tag{23}$$

Appendix A.5 for vector k defining in three dimensions $k_x=2\pi N_x/L;\ k_y=2\pi N_y/L;\ k_z=2\pi N_z/L;\ Nx,Ny,Nz=\pm1,\pm2,\pm3,\cdots$ are solutions for the vector A, in terms of unit vectors $\widehat{e_{k\rho}}\ \exp(\pm ik\cdot\rho)$ where $\widehat{e_{k\rho}}$ defines the unit vector. Here, unit vectors satisfy $\widehat{e_{k\rho}}.\widehat{e_{k\rho'}}=\delta_{\rho\rho'}$ also $k.\widehat{e_{k\rho}}=0$. These two-unit vectors are known as polarization vectors representing polarization properties of radiation. The solution $E_{k\rho}=\widehat{e_{k\rho}}\exp(\pm ik\cdot\rho)$ are orthogonal vectors satisfying the property $(1/V)\int_V\psi_{k\rho}.\psi_{k'\rho'}=\delta_{kk'}\delta_{\rho\rho'}$. These wave vectors are Laguerre Gauss (LG) modes defining the helical waves carrying OAM modes which are all orthogonal modes [12]. Two waves travel perpendicular to the direction of propagation k defined by $e_x\,e_y$. Unlike other particles, the spin states of a photon are mapped to the classical aspect of light. Total angular momentum is given by [5, 41] $L=(l+\sigma)\hbar$. Laguerre Gaussian Index, $\sigma=$ (linearly polarized) $\pm$ (circularly polarized), forms helical structure of beams [5, 7]. Laser field spatially modulates the electrons in a helical pattern. For a circularly polarized wave $\sigma=\pm1$, for right and left circularly polarized light and angular moment is defined by $\iota\hbar$ and spin angular moment by $\sigma\hbar$. Azimuthal component of light's linear momentum is also defined as per photon. Angular momentum operator and its representation in spherical polar coordinates [38] are defined by spin states of photons which generate quantum states. Let spin operator be defined by $M=M_1e_1+M_2\,e_2+M_3e_3$ where its components have commutation relation $\{l_i,l_j\}=\{i\hbar\epsilon_{ijk}l_k\}$ where ϵ_{ijk} is the Levi-Civita symbol [42] and $[M^2,M]=0$.

Forming a common eigen basis component l_i,

$$\text{For spin states}\ L_z|l_1m>=\mathrm{m}|l_1m>. \tag{24}$$

For every azimuthal component $l=0,1,2,\cdots,m=-l,-l+1,\cdots,l-1,l$ [34, 43] in Helmholtz equation.

The quantum number M is empirically fixed at a single half integer. States of a particle in common basis $\{\mathrm{m}>\otimes M\}$ will be described as

$$\left|\varphi>=\sum_{m,M}C_{m,M}|n>\otimes|l>.\right. \tag{25}$$

A communication link is set by the stream of particles between two locations. Here, modulation is done in the spin state in a chosen axis. The particles also acquire an orbital angular momentum (OAM) in addition to spin. Spin component is in the direction of propagation $e_k=k/k$ which is compatible to the momentum operator $p=k\hbar$. For $m=0$, there is no eigenstate. It is a solution to the field equations, for $n=1$ and -1; there are two spin states [8, 9]. Hence, probability of finding a particle from 0 to radius ρ in terms of its energy is

$$\int_0^\rho p(x)dx=\left(\sqrt{2m\,E_{n'}}\right)\rho. \tag{26}$$

If in the calculation of polarization parameter

$$\begin{aligned} &e=\exp(i\varphi\pm n),\\ &[e,p]=e,\\ &e=\sum_{m=0}^{\infty}|m,l><m+1,l|,\\ &e-=|m,l>=|m-1,l>,\ e+|m,l>=|m+1,l>\ [44]. \end{aligned} \tag{27}$$

Appendix A.6 in LG modes, the eigenstates of the spin operator are the circular polarizations; hence, the description of $|M>$ will include spin state. Spin is defined as polarization vector given by [34, 43]

$$m_{np}=(c_+\,e_+)+(c_-\,e_-)\ \text{where}\ |c_+|^2+|c_\pm|^2=1, \tag{28}$$

where the polarization states as $e_-\gg|-1>$ and $e_+\gg|+1>$.

Writing for a common basis of spin and OAM,

$$\left|M>=\sum_{S=-1,1}\sum_{n=-\infty}^{\infty}\sum_{m=0}^{m=\infty}c_{nmM}\right|n,m>\otimes|S>. \tag{29}$$

This serves as the basis of a potential communication [41] scheme. In quantum communication, quantum bits are assigned to the spin states, and additional information is assigned to the OAM quantum number and associated radial number m.

2.2. Scattering Matrix. Jones matrix J [44] gives the scattering matrix. Polarization states of the scattered wave connected to that of incident wave

$$\begin{bmatrix} E_x^{\,s} \\ E_y^{\,s} \end{bmatrix} = \begin{bmatrix} J_{xx} & J_{xy} \\ J_{yx} & J_{yy} \end{bmatrix} \begin{bmatrix} E_x^{\,i} \\ E_y^{\,i} \end{bmatrix} = J^l \begin{bmatrix} E_x^{\,i} \\ E_y^{\,i} \end{bmatrix}. \tag{30}$$

To generate OAM, geometric phase is used to generate $e^{il\varnothing}$ of an OAM wave. The OAM scatterer is generated by a metasurface with azimuthal location $\varnothing$. It provides a phase change of $l\varnothing$. $J_{yy} = -J_{xx} = \mp 1$ and $J_{yx} = J_{xy} = 0$. Cocircularly polarized components are filtered, and a cross-circularly polarized component carries OAM. The polarization of vector fields is [44] controlled by a linear polarizer. If an incident wave is circularly polarized, i.e., $E^{\mp} = 1/\sqrt{2}[1 \mp i]^T \pm$ sign for LHCP and RHCP, respectively, the output wave is having a geometric phase of $e^{\mp i\alpha}$ [34].

3. OAM Modes

3.1. OAM Modes Generation by High Order Hermite–Gaussian Modes (HGMs). Detail analysis is done for these OAM modes mathematically. Laser modes are generally Hermite–Gaussian [34]. The electric field distributions here are mutually orthogonal [38]. Linear harmonic oscillator using one dimensional Schrodinger wave equation is studied to understand the quantum mechanical behavior of atoms for their coherence states [38]. The Mach–Zehnder interferometer model is used for square Hermite–Gaussian Vortex pulse beam [43]. $HG_{n,n}$ modes from optical tweezers are used to generate bright spot high order HGM [38, 43] in 2D arrays. In the coherent state, angular momentum is transferred to micro particles or an atom which represents the modes of an optical resonator. These modes are simulated in pumped solid-lasers [43]. Arbitrary field distribution can be decomposed in this form [38]. The Hermite–Gaussian functions are orthogonal sets of functions [43].

3.2. Mathematical Presentation of HGM Waves. The following mathematical equation represents high order HGM distribution [34, 38, 43]:

$$\begin{aligned} \cdot HG_{n_x,n_y}(x,y,z) &= \left(\frac{1}{2^{n_x+n_y-1}\pi n_x! n_y!}\right)^{1/2} \frac{1}{W_z} \times H_{n_x} \\ &\cdot \left(\frac{\sqrt{2}x}{W_z}\right) H_{n_y}\left(\frac{\sqrt{2}y}{W_z}\right) \exp\left(-\frac{r^2}{{W_z}^2}\right) \\ &\cdot \times \exp i\left[Kz + \frac{Kr^2}{2R_z} - \left(n_x + n_y + 1\right)\varphi_G(z)\right], \end{aligned} \tag{31}$$

K is the wave number, W_z is the beam width, R_z is the curvature radius of phase front, Z_R is Rayleigh length, and $H_n(.)$ n is the order of Hermite polynomials, respectively.

Phase is given by $\psi_G(z) = \tan^{-1}(z/z_R)$.

$HG_{n,n+1}$ and $HG_{n+1,n}$ modes are superposing with $\pm\pi/2$ phase difference which forms resultant superposed beam $n^2 + (n+1)^2$ vortex. They are aligned in a square manner. The effect of $\pi/2$ phase difference between the two subbeams introduces a coefficient i between two superposed subbeams. Resulting square vortex laser beams in the resonator are observed by changes in the phase and intensity profile [34, 43] given by

$$HG_{n,n+1} \pm i \times HG_{n+1,n}. \tag{32}$$

Experimental lasing is given by $HG_{n,n}$ mode patterns. $n \times n$ bright spots of $HG_{n,n}$ modes are in an array manner. The x and y axes are defined by

$$H_n\left(\frac{\sqrt{2}x}{W_z}\right) H_{n+1}\left(\frac{\sqrt{2}y}{W_z}\right) + i \times H_{n+1}\left(\frac{\sqrt{2}x}{W_z}\right) H_n\left(\frac{\sqrt{2}y}{W_z}\right) = 0. \tag{33}$$

Since Hermite polynomials have real values, there are n^2 cross-section points of x nodal lines of $HG_{n,n+1}$ mode and y nodal lineof $HG_{n+1,n}$ mode [34, 38]. Solution of equation is $(n+1)^2$ cross-section point of y nodal line of $HG_{n,n+1}$ mode and x nodal line of $HG_{n+1,n}$ mode.

High-order HGM lasing and another higher-order HGM lasing are easily achieved. Generations of helically phased beams HG01 and HG10 are combined to give optical vertices [45]. Fundamental Gaussian mode can be converted to helically phased mode using laser. Holographic approach is used with spatial light modulators (SLMs). These SLMs are pixelated liquid crystal devices programmed through a computer. A telescope is also used to transform Hermite–Gaussian (HG) and LG modes. π converters and $\pi/2$ converters, which are also called $\lambda/4$ and $\lambda/2$ plates [45], are used to transform HG to LG modes. These optical devices have many more advantages over holograms.

3.3. Different Vortex Beams and the Difference. Different types of OAM carry OAM waves in free space are L.G. beam, Hermite (HG) beams, Bessel beams, hypergeometric beam, hypergeometric-Gaussian beam, and other beams [38]. OAM beams in free space can be mixed using different modulation schemes [38]. Many methods have been suggested [15] such as photonic crystal fiber (PCF) structure with rectangular air holes [46] and Bessel polygon air holes. Studies found that circular air holes and noncircular air holes in photonic crystal fiber support Bessel polygon, which has very low confinement loss in order of 10^{-10} dB/m. PCF combining different sizes of air holes are also suggested [33].Ring core fiber [33] is supposed to have good performance characteristics for OAM modes in wired communication. Several schemers for generating the OAM output are suggested [33]. OAM with quantum entanglement properties have infinite number of Hilbert space all orthogonal basis. PCF (photonic crystal fibers) and RCF (ring core fiber) are mainly being used to generate OAM.

The oceanic turbulence Geometric Gaussian (HGG) vortex beam is also analyzed with different wavelengths [45]. In underwater optical communication (UOC), HG are separated as Gaussian mode, modified exponential Gaussian mode,

modified LG mode, and modified Bessel's mode [47]. In underwater communication, OAM is of more interest because it has higher multiplexing capacity. Angular momentum cross-talk is reduced in case of underwater communication when it is Bessel Gaussian beam and hypergeometric Gaussian beam [29, 47].

Hypergeometric-Gaussian beams are to be discussed in case of wireless communication. By a computer-generated hologram, we can generate hypergeometric OAM and LG beam with different radial indices (Figure 1). Enhanced learning capabilities are introduced in the model to train a convolutional neural network. Manipulation of OAM through hologram is becoming more of an interesting topic nowadays. Hypergeometric beams have the properties of auto focusing and diffraction-free communication mode.

Another frequently used mode family is L.G. modes, which are based on polar coordinates. L.G. mode fits more in the situations where there is rotational symmetry.

OAM is susceptible to atmosphere turbulences, so there is a need to study scan diffracting beams which are found other than LG Modes. OAM techniques are analyzed in both classical and new quantum regimes. OAM waves can be generated by a hologram in both classical and quantum states. OAM states are characterized by OAM numbers $\{\pm 1, \pm 3 \pm 5\}$. It is also described by quantum walk. In this paper, OAM waves are described by the Helmholtz equation. Hypergeometric beam is also known as Bessel's Gaussian beam is a pseudo-non-diffracting beam family [48]. The mathematical derivation is also explained in Section 2. The beams have autofocusing property, larger angular momentum, and self-reconstruction after an obstacle. It has great potential for wireless optical communication [28, 29]. In atmosphere turbulence [48], hyper-Gaussian beams [48, 49] are purposed to work strongly through moderate to strong anisotropic conditions. Anisotropy is present in the atmosphere with a layer up to 25 km or in high altitude of the stratosphere. The wireless communication using OAM will be the future study area where Bessel's and the hypergeometric wave function will be focused for atmosphere turbulence and other under water communication.

3.4. OAM Constellation Conventional Approach and Modification/Improvement. Generation and detection are done in earlier experiments [21] using the Dammann optical vortex gratings (DOVGs). For beam generation, OAM beam diffraction grating is used.

$$\text{If } A = \exp(i\varnothing) = \sum_{-N/2}^{N/2} E_N \exp\left(\text{in}\,\frac{2\pi X}{T} + l\theta\right), \tag{34}$$

where $\varnothing$is a phase function, T is the grating period, N is diffraction order from $-N/2$ to $N/2, \theta$ is the azimuthal angle in polar coordinator, l is the interval of the topological charges, and $\lceil {E_m}^2 \rceil = 1/N$ is the power of nth order normalized with respect to total power.

Micro-ring-based OAM devices are used to decode the OAM. This is also known as optical coded division multiple access (OCDMA). Here, OAM value is used as an address code of each node value. Suitable OAM transmitters and detectors enable flexible and dynamic function for multiplexing [20].

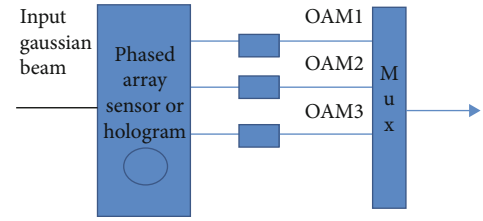

Figure 1: Modulation multiplexing scheme using hologram and phased array sensor in OAM.

3.5. Hermite–Laguerre–Gaussian Modes. Hermite–Laguerre–Gaussian modes with elliptical vortices are the LG modes. These modes are defined by Appendix A.8.

$$HLG_{n,m}\left(r, \frac{z}{\alpha}\right) = \frac{1}{\sqrt{2^{N-1} n! m!}} \exp\left(-\pi \frac{|r|^2}{W}\right) HL_{n,m}\left(\frac{r}{\sqrt{\pi}}\ \frac{}{W}\middle|\alpha\right), \times \exp\left[iKz + iK\frac{r^2}{Z_R}\right] - i(m+n+1)\theta, \tag{35}$$

where $HL_{n,m}(\cdot)$ is a Hermite Laguerre Polynomial.

$$r(x,y)^T = (r\,\text{Cos}\,\varphi, r\,\text{Sin}\varphi)^T, \quad R(z) = \frac{\left({Z_R}^2 + Z^2\right)}{Z}, \quad Kw^2(z) = \frac{2\left({Z_R}^2 + Z^2\right)}{Z_R}, \tag{36}$$

where $\theta(z) = \tan(Z/Z_R)$ and Z_R is Rayleigh range.

For $\alpha = 0$ or $\pi/2\ HLG_{n,m}$, mode is reduced to $HG_{n,m}$ or $HG_{m,n}$ mode.

For $\alpha = \pi/4$ or $3\pi/4$ the $HLG_{n,m}$, mode is reduced to $L\,G_{p,\pm l}$ mode $[p = \min(m,n)\ l = m - n]$ [30].

$LG_{p,l}$ mode can be decomposed into a set of Hermite–Gaussian (HG) modes.

An earlier experiment on OAM used 28 GHz with 1 GBaud/s signals with 16-QAM modulation. 32 Gbit/s is obtained by employing 4 different OAM modes for $l = -3, -1, +1$, and $+3$ on two orthogonal linear polarization states [30]. OAM beams are generated by Gaussian beams which passes through a spiral phase plate [30]. An inverse spiral surface in SPP can convert an OAM beam back into a Gaussian beam. These SPP are made of high-density polyethylene (HDPE) (Figure 2) which has a refractive index of 1.51 at 28 GHz. The OAM beams are generated from the interference patterns between each OAM beam and the Gaussian beam, which are combined through a beam splitter [35].

New wave equation consists of spherical eigenvalues with individual wave consisting of spherical waveform, equation in form of eigenvalues [51], where l lies $-l < m < l$ in waveform

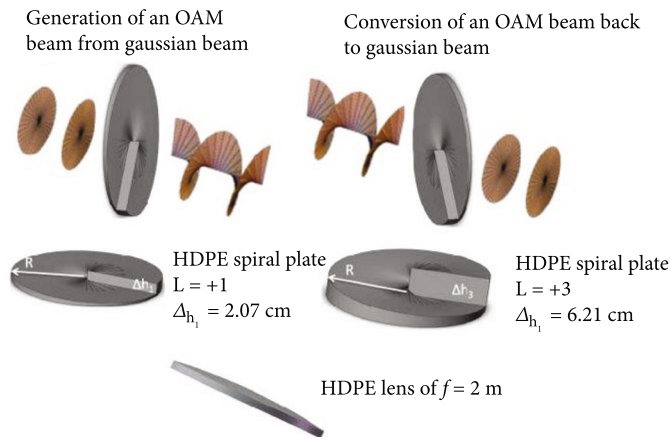

Figure 2: OAM generation by HPDE spiral plate [Figure 2, 35].

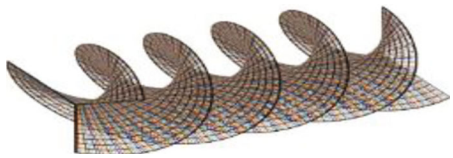

Figure 3: Helix wave pattern in OAM wave [Figure 2, 51].

generator. These HG modes are plotted [51] in Figures 3 and 4.

$$
\begin{aligned}
Y_{0,0} &= \frac{1}{(4\pi)^{1/2}},\\
Y_{1,0} &= \sqrt{\frac{3}{4\pi}}\cos\theta,\\
Y_{1,1} &= -\left(\sqrt{\frac{3}{8\pi}}\right)\sin\theta e^{+i\varphi},\\
Y_{2,0} &= \left(\sqrt{\frac{5}{16\pi}}\right)\left([3\cos\theta]^2-1\right),\\
Y_{2,1} &= -\left(\sqrt{\frac{15}{8\pi}}\right)\sin\theta\cos\theta e^{+i\varphi},\\
Y_{2,2} &= \left(\sqrt{\frac{15}{32\pi}}\right)(\sin\theta)^2 e^{+2i\varphi},
\end{aligned}
\tag{37}
$$

Finally, the wave patterns of HE and EH modes are combined to generate OAM waves. $\mathrm{OAM}_{l,m}$ modes obtained by vector mode superposition [52, 53] are represented in the form of l, m as follows:

For $l > 1$

$$
\begin{aligned}
\mathrm{OAM}^{\mp}_{\mp l,m} &= \mathrm{HE}^{\mathrm{even}}_{l+1,m} \mp j\mathrm{EH}^{\mathrm{odd}}_{l+1,m},\\
\mathrm{OAM}^{\mp}_{\mp l.m} &= \mathrm{EH}^{\mathrm{even}}_{l-1,m} \mp j\mathrm{EH}^{\mathrm{odd}}_{l-1,m}.
\end{aligned}
\tag{38}
$$

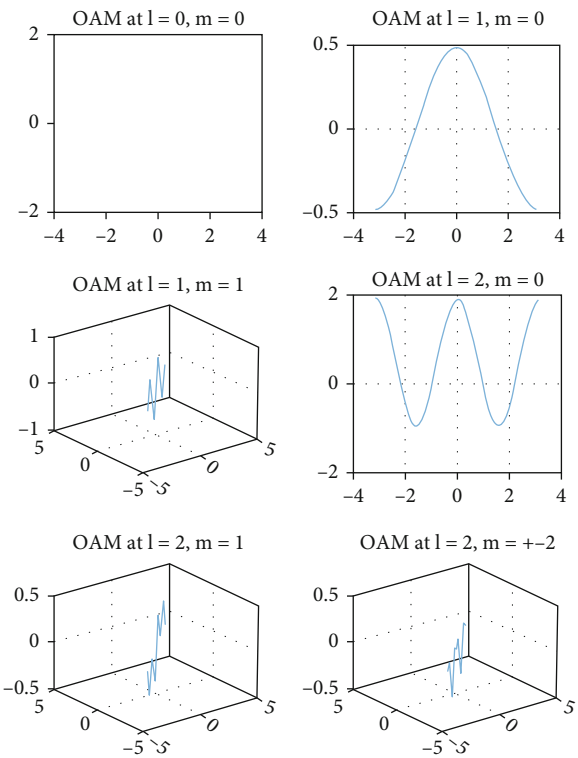

Figure 4: OAM wave generation [Figure 1, 51].

For $l = 1$

$$
\begin{aligned}
\mathrm{OAM}^{\mp}_{\mp l,m} &= \mathrm{HE}^{\mathrm{even}}_{2,m} \mp j\mathrm{HE}^{\mathrm{odd}}_{2,m},\\
\mathrm{OAM}^{\mp}_{\mp l,m} &= \mathrm{TM}^{2,m}_{0,m} \mp j\mathrm{TM}^{2,m}_{0,m}.
\end{aligned}
\tag{39}
$$

These waves are represented in the form of TE modes, TM modes, and mixed wave modes (HE, EH).

3.6. Effective Refractive Index Difference, Confinement Loss, Mode Purity, and Isolated Parameters. OV (optical vertex) has OAM lh per photon; l is topological charge, h is the reduced plank constant. OV mode for $l = \mp 2$ has been experimentally

proposed in a four-mode fiber.

$$OV_{\mp} = LP_{lm}^{\text{even}} \mp iLP_{lm}^{\text{odd}}. \quad (40)$$

$OV_{\mp 2}$ mode is composed of $LP_{21}^{\text{odd}} \mp LP_{21}^{\text{even}}$ with $\mp(\pi/2)$ phase difference. LP_{01} is converted to other modes. The spatial phase form of $\exp(il\varnothing)$ ($l = 0, \mp 1, \mp 2, \cdots,$) gives OAM an infinite number of orthogonal eigenstates.

LG modes also increase spectral efficiency [54, 55] and information carrying capacity. Moreover, OAM provides better security. OAM can facilitate many application areas, so it is of great importance.

In case of photonic circuit fibers used for OAM generation, it is found that circular shaped photonic crystal fiber supports several OAM modes [53] of 1000 nm bandwidth. Each OAM confinement loss is 10^{-9} to 10^{-8} db/m for this fiber. Crystal fibers with square and circular air holes [52] also support OAM. Confinement loss is less for these fibers. In these fibers, different modes have different propagation constant β. The relationship between n_{eff} and β can be expressed as

$$n_{\text{eff}} = \frac{\beta}{K_0}. \quad (41)$$

$K_0 = 2\pi/\lambda$, K_0 is the wavenumber in the vacuum, and λ is the wavelength. ERI (effective refractive index) [52] decreases faster with the increase in a mode order. ERI increases as wavelength increases. To avoid coupling between modes, ERID should be greater than 1×10^{-4}[52].

PCF supports 70-80 OAMs and LP modes (linearly polarized modes) [53, 56, 57].

Good propagation features possess using PCF supports better mode quality (96%) and good isolation value about 72db that gives low crosstalk between [56, 57] guided channels. OAM covers 1520 to 1630 nanometer whole L band and C band [37, 57, 58].

Confinement loss in PCF is given in equation (42) [54] which is induced by the light absorption inside fiber:

$$C_{\text{loss}} = \frac{40\pi}{\ln(10)\lambda} I_m(n_{\text{eff}}) \left(\frac{\text{dB}}{\text{m}}\right). \quad (42)$$

λ is the operating wavelength, and $\text{Im}(n_{\text{eff}})$ is the imaginary part of refractive index (RI). PCF properties in terms of RI are

$$n^2(\lambda) = 1 + \sum_1^3 \frac{A_i\lambda^2}{\lambda^2 - {\lambda_i}^2} \text{ [53]}. \quad (43)$$

${\lambda_i}^2$ and A_i are Sellmeier coefficient, and $n(\lambda)$ is the RI that varies with wavelength. ERID is effective refractive index difference.

$$\Delta n_{eff} = \left| n_{\text{eff}} HE_{l+1,1} - n_{\text{eff}} EH_{i-1,1} \right| > 10^{-4}, \quad (44)$$

$R\,|n_{eff}|$ is real part of RI. 38 OAM modes are supported by above mentioned PCF (wavelength 1000-2000 nm). Fused silica gives the best results in terms of low dispersion, it has lower ERID.

Light is guided between center air holes and holes in cladding. Zhang et al. proposed a scheme of C-PCF (26 OAM). Jia et al. proposed hollow core ring PCF supporting 38 OAM modes. Lower order modes show less dispersion. Higher order modes have dispersion. So lower order modes [23, 24] are stronger for stable fiber communication. Small confinement loss is necessary for robust and efficient transmission of light in fiber. A lower nonlinear coefficient is advantageous for transmitting the OAM mode into optical fibers. Reports of various PCF find circular for 100 nm and 1000 nm BW, spiral for 600 nm BW, and double for 850 nm BW, with very low confinement losses 10^{-7} to 10^{-9} dB/m. PCF for 76 OAM modes [56] is designed with 6 linear polarizations. OAM beams are used in MDM [23–25] which enhances transmission capacity. OAM has been used for optical manipulation and imaging. These designs have been proved using COMSOL multiphysics simulating software.

In terms of em field $E(x,y)$, an effective area is given by

$$A_{\text{eff}} = \frac{\left(\int |E(x,y)|^2 dx\, dy\right)}{\left(\int |E(x,y)|^2\right) dxdy}. \quad (45)$$

The following is the numerical aperture:

$$\text{NA} = 1 + \frac{A\, A_{\text{eff}}^{-1/2}}{\pi^2}. \quad (46)$$

Dual guided photonic crystal fiber supports large capacity transmission [54] in high speed optics communication with LP modes. Twisted fibers, SPP, cylindrical lenses, helical lattices, twisted hollow core fibers, and step index fibers have been used for OAM transmission.

Dispersion in fibers is given by

$$D = \frac{-\lambda}{c} \frac{d^2 R[n_{\text{eff}}]}{d\lambda^2}. \quad (47)$$

In this equation, $R(n_{\text{eff}})$ is the real value of the effective refractive index, and c is velocity of light.

Nonlinear property of PCF is expressed as [54] $\gamma = 2\pi n_2/\lambda A_{\text{eff}}$, where n_2 is the nonlinear coefficient of fused silica $n_2 = 2.6 \times 10^{-20}$ m^2/W.

4. Effect of Atmospheric Turbulence on Optical Signal Propagation

OAM modes suffer loss of information in atmospheric turbulence due to intermodal dispersion in fibers and higher order modes. 850 nm VCSEL has been used for OAM generation [59]. It is used with multimode fibers (MMF). Optical beam-carrying multiplexed OAM is directly transmitted to an atmospheric channel (Figure 5) from the fiber termination point. Atmospheric turbulence affects the signal at the receiver side optical beam is directly focused to the second MMF core [59]. Hence, this setup is used for short distance communication. Hybrid FSO communication links do not

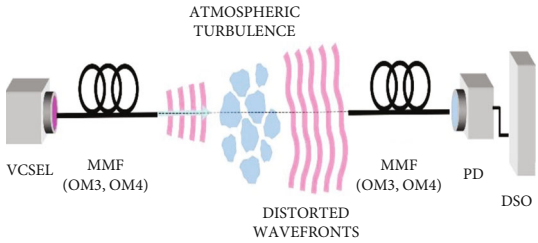

Figure 5: Fiber hybrid fiber—FSO system.

require costly electric to optical and optical to electrical signal converters, and no amplification stages are needed before transmitting and receiving through the atmospheric channel.

10 GHz Ethernet is applied using this technology for LAN [59], and it can be used for metronetwork and enterprise connectivity broadband heterogeneous wireless services. It is also being used as an extension of radio over fiber link [59]. Phase distortions are caused due to turbulence which is the reason for intermodal cross-talk [2]. It can be reduced if the phase front of an OAM beam is partially adjusted. An experiment reports [2] adaptive optics techniques to mitigate the effect of atmospheric turbulence.

In a random medium such as the atmosphere, ocean, and tissue, optical beam intensity fluctuates in the propagation paths [45]. Scintillation is caused by temperature variations in the random medium, which results in index-of-refraction fluctuations. This is also known as optical turbulence. [60] OAM can be used high-definition video broadcasts, video conferences, distance education, and webcasts, which demand increased network capacity. Laser beams are expected to be the next generation communication tool, having large-capacity for satellite, ground, and unmanned aerial vehicles (UAV) using spatial propagation. This has also advantages of reduced size and weight of optical terminals.

In oceanic communication spatial correlations, Kolmogorov power spectrum is a method used to analyze the atmospheric effect [45]. Backward scattering method is also used for OAM analysis in turbulent atmosphere [61]. Scintillation index reduces with the increase of the topological charge it makes OAM beam, propagating longer distances [45], but mode scattering increases for higher order modes. Angular momenta is conserved for the free-space propagation [62] but not for an inhomogeneous medium. Scintillation severely impacts the operation of target designation [63] experiments done on the model simulations of discontinuity of statistical variations of atmospheric conditions. For geometrical optics, Monte Carlo simulations are done for the statistical [63] models. A multibeam reduces the effect of the atmospheric turbulence. The multibeam is obtained by [60] a mirror and a beam splitter using laser and telescope. For turbulent-free space communication, OAM with 4 channels [23] has been proved experimentally using WDM/SMM technique at 1550 nm wavelength.

High-order Bessel beams also have an advantage of OAM in multiplexing FSO communication. Wide-spectrum lasers reduce Scintillation effects. Supercontinuum decreases atmospheric turbulence. For this, wide-spectrum OAM beams are used. In weak turbulence channels, the performance is measured by SI, PF, and BER [64]. Fog, dispersion, absorption, rain, and snow [65], these are the range-limiting factors in atmospheric communication which is called atmospheric turbulences. In wired and space communication, lasers of 1550 nm wavelength have lower optical losses than 830 nm wavelength. Atmospheric turbulence is governed by the Navier–Stokes equations; the statistical approaches are developed to solve this. OAM beam patterns do not change during the propagation in atmospheric turbulence, and it evolves into a Gaussian beam as propagation distance increases. After propagating 1000 m, beam array transforms into a fan structure in moderate turbulence; then, it turns to a single vortex beam after propagating 5000 m. Also, optical vortex beams are able to propagate longer distances in weak turbulent atmosphere. When distance exceeds 500 km, the output beam finally loses the OAM property and gradually becomes a Gaussian-shaped beam. Scintillation affects more to the LG vortex beams.

5. Experiments

Figure 6 shows the experimental setup of VCSEL converting bit stream into an OAM wave. A spatial analyzer is used to measure the OAM wave.

These OAM waves carry the random data which we use to multiplex them. Similarly, at the receiving end, the demultiplexed data are obtained. Figures 5 and 7 show the transmission link for OAM waves. In our photonic circuit, VCSELs are used for generating twisted light beams (Laguerre–Gaussian laser beams). VCSEL (vertical surface emitting laser) is a multimode transmitter; it has inbuilt spatial light modulator or multimode generator by changing the parameters of the LG mode expression, both SAM and OAM of a photon beam [39] can be visualized. Different modes with different azimuth and different radial component are generated using VCSEL which are shown in Figure 8. The wave has a corkscrew pattern [1, 2, 5] of the scalar field. Optically dense and white lines are observed. Modes are generated for intensity profile of $n = -1, 0, +1$. Doubled parabolic light energy curves are shown representing different radial modes $m = 0, 1, 2, \cdots$

At $n = 0$, it shows a Gaussian beam [10]. For experiments, the wavelength of light is taken as 1550 nm.

Pseudorandom pulses [6, 12] and user-defined bit sequences drive VCSEL which generates light beams of OAM. The following results are obtained in simulations.

5.1. Case 1: OAM Wave Generation by VCSELs of Same Wavelength (Appendix A.8). Using light of single wavelength 1550 nm in VCSEL, the following modes are observed by varying spin quantum numbers and azimuthal quantum numbers: $m = 0$, $n = 1$ (Figure 8(a)); $m = 1$, $n = 1$ (Figure 8(b)); $m = 2$, $n = 1$ (Figure 8(c)); (d) $m = 3$, $n = 1$ (Figure 8(d)); $m = 1$, $n = 2$ (Figure 8(e)); and $m = 2$, $n = 2$ (Figure 8(f)).

These OAM modes are being generated by individual lasers separately. So we can use each OAM to send information through the fiber. Fibers carrying these are multimode fibers. Linearly polarized light is converted to spherically polarized light by VCSEL, and multiple modes of OAM are

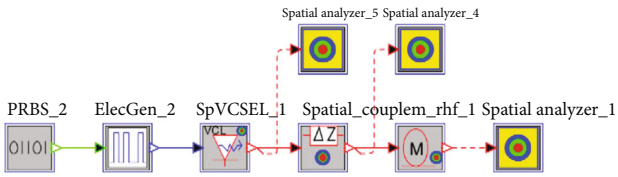

(a)

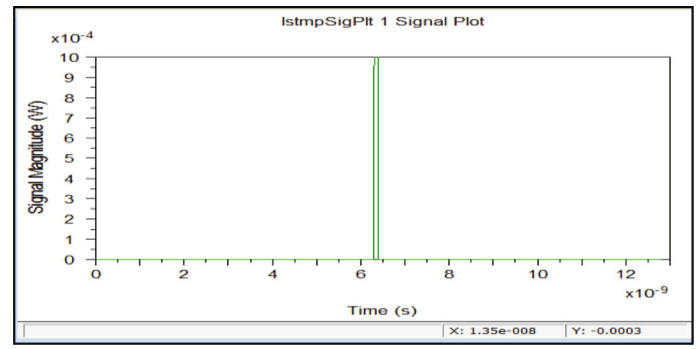

(b)

Figure 6: (a) Experimental setup for OAM generation by single VCSEL. (b) Laser power in milliwatt.

generated. To check the modes again, spatial analyzers are used.

5.2. Case 2: OAM Wave Generation by VCSELs of Different Wavelengths. With a single VCSEL, we generate OAM waves of different wavelengths as shown in Figure 9.Wavelengths from 1550 nm to 1560 nm are used at a wavelength difference of 5 nm. Each input wavelength is varied, which is at a difference of 5 nm to the laser. At 1550 nm, outputs in the form of intensity profile are shown in Figure 9(a) ($m = 3$, $n = 3$), at 1555 nm output by Figure 9(b) ($m = 4$, $n = 1$), at 1560 nm Figure 9(c) ($m = 4$, $n = 2$), and at 1570 nm ($m = 3$, $n = 3$) Figure 9(d). Figures 9(a)–9(d) show modes for $m = 3$, $n = 3, 4$; $m = 3$, $n = 1, 4$; $m = 4$, $n = 2, 4$; and $m = 3$, $n = 3$, respectively.

Figures 8 and 10 show intensity profile of beam diffracted from SLM (modulator) emitted by VCSEL integrated SPPs by $l = 0, +1, +3, \cdots$, up to so on. l is the helical wave front of OAM beam. Higher topological charge gives larger diameter of annular far field. It gives scope for free space quantum communication.

Figure 11(a) shows OAM waves carrying 0.3 to 3 m V of the OAM generated by different wavelengths. Power used by the four OAM waves in multiplexing is shown in Figure 11(b). Experiments show that OAM waves consume almost zero power in multiplexing. Power of different baseband signals being modulated by these OAM waves is shown in Figure 12(a).

5.3. Multiplexing. Multiple waves of OAM are multiplexed as shown in Figure 7. These waves are multiplexed using 1550–1570 nm laser waves at a difference of 5 nm (1550 nm, 1555, 1560, and 1565 nm). OAM number in spin and azimuth can be calculated by their rings and centers in pair marked in red color as shown in Figure 9 showing m (spin quantum number) and n (azimuth quantum number). Maximum power shown is 0.25 milliwatt. Four signals are multiplexed with the spatial mode using four input ports. Keeping the radial component as1and azimuth component as 0,1,2,3, a multimode fiber carries spatial modes without much dispersion [2, 5, 12]. Figures 10(a) and 10(b) show the multiplexing [42] of these modes with power spectrum. LP modes were multiplexed [12, 13] and sent through the photonic circuit. Laguerre Gaussian (LG) beam is the most common optical vortex beam [8, 42]. For multiplexing of N information carrying OAM, beams are given by

$$\Psi(\rho,\varnothing,\mathrm{t}) = \psi_n(t).\psi_n(\rho).\exp\,(il_n\varnothing), \quad n = 1, 2, 3, \cdots, N. \tag{48}$$

The resultant field is given by

$$\psi_{mux}(\rho,\varnothing,t) = \sum_{n=1}^{N} \psi_n(t)\psi_n(\rho).\exp\,(il_n\varnothing). \tag{49}$$

Positive SAM state can be obtained by combining the OAM waves. Figure 10(c) shows the wavelength division multiplexing all wavelengths of equal power, and the wavelengths are generated at a nanometers. The waves are modulated by using four baseband signals of low frequency input signals. Power used is almost zero as shown in Figure 10(b). Signal magnitudes of multiplexed wavelengths are of 0.0025 W. After multiplexing, the total power is also shown by the simulation in Figure 11(b). Signal eye diagram presents signal variation between 0 and 0.2 m V in 10 GHz range. These baseband signals obtained are of very low power as shown in dBm Figure 12(a). Signal output shown in the eye diagram has maximum output of 1.5 V. Figure 12 is the complete multiplexed OAM signal and the corresponding output power in dBm [66]. OAM multiplexing enhances the performance of the multiuser system of these channels [31, 32]. Output after demultiplexing power spectrum of different baseband signals was achieved as shown in Figure 12(a). Figure 11(a) shows amplitude of multiplexed wavelengths. Figure 10 shows that if we increase the OAM waves, the output power consumed decreases. Hence, in optical networks, higher numbers of OAMs give better results as almost OAM waves carrying information at zero power is consumed.

If we compare with other techniques, there is no power analysis so far has been seen in case of OAM generated by planar antennas using PCBs and also holographic techniques. Although we have a portable OAM devices using PCBs, it needs extra hardware for test. PCB technology lags

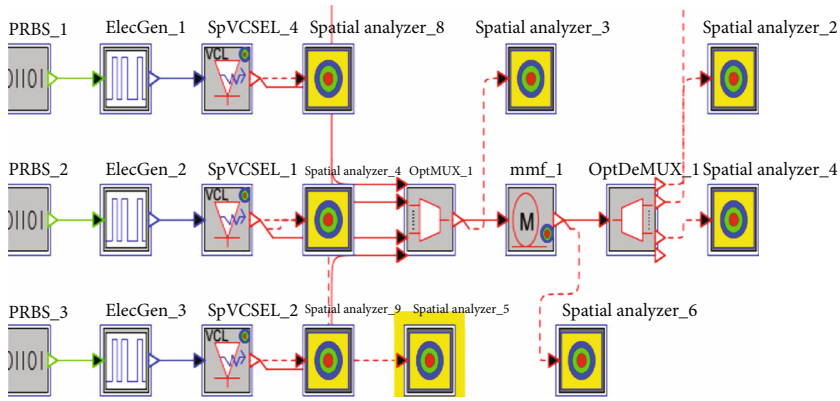

Figure 7: Wavelength division multiplexing/demultiplexing using VCSELs with OAM.

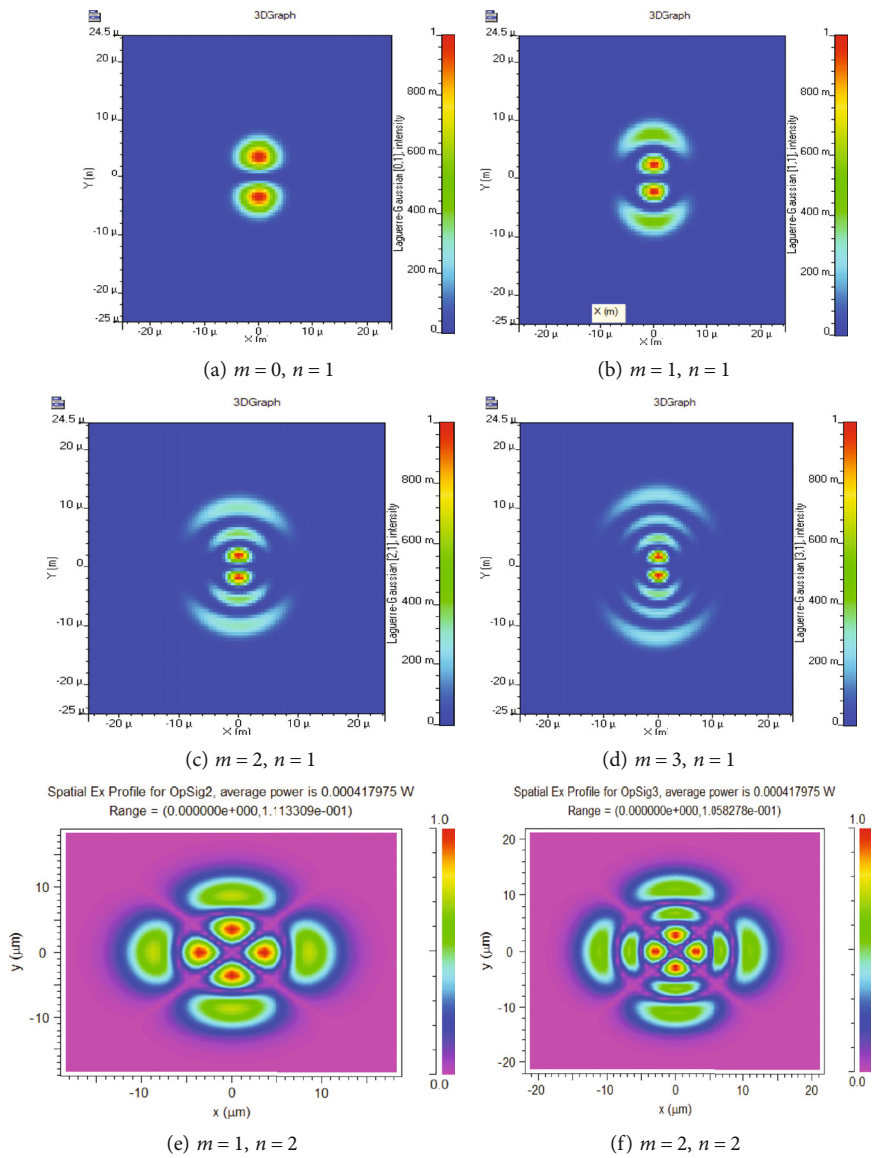

(a) $m = 0$, $n = 1$ (b) $m = 1$, $n = 1$

(c) $m = 2$, $n = 1$ (d) $m = 3$, $n = 1$

(e) $m = 1$, $n = 2$ (f) $m = 2$, $n = 2$

Figure 8: VCSEL modes for different values of azimuth and spin quantum number.

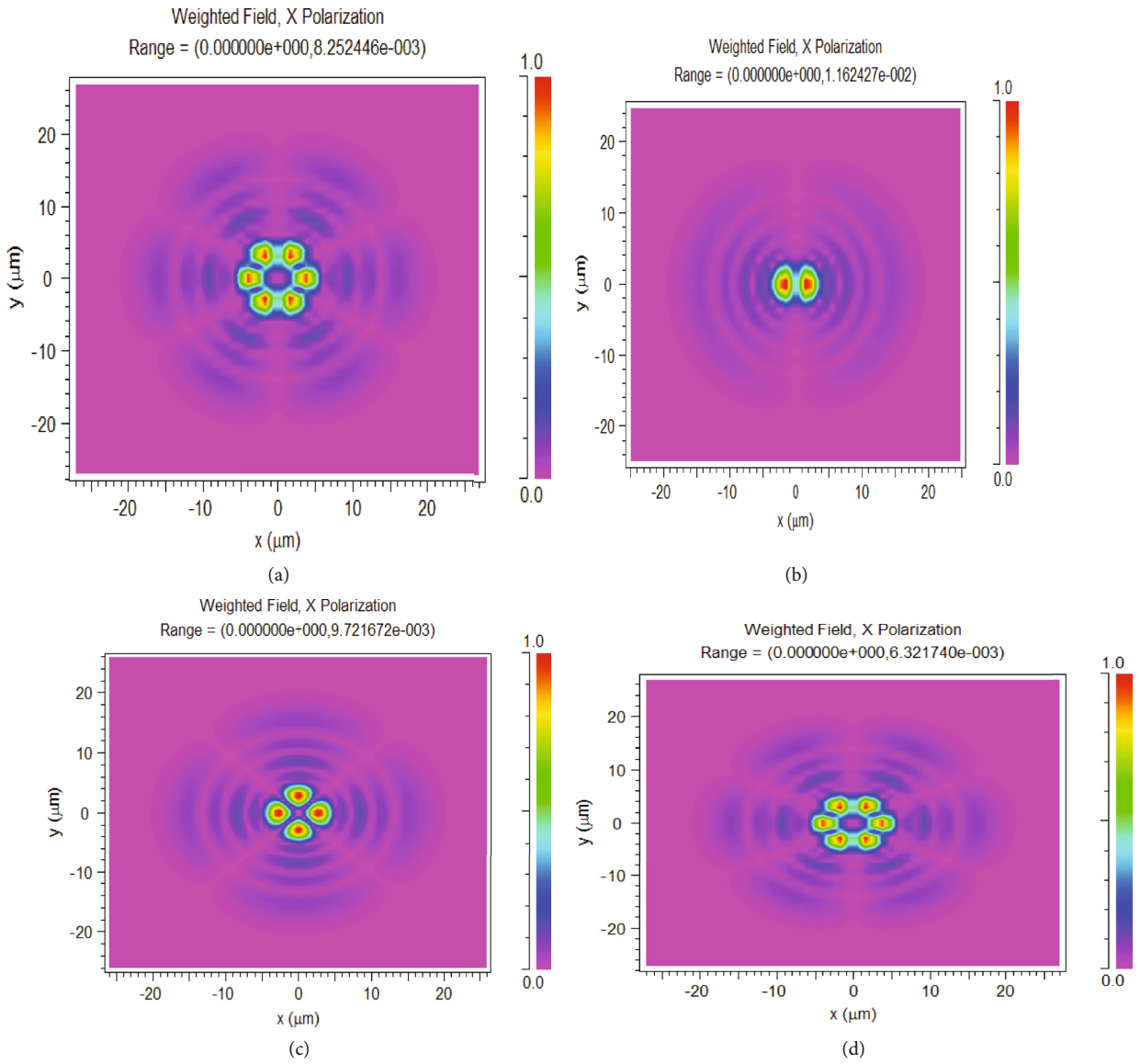

Figure 9: OAM waves of different wavelengths having different azimuth and spin numbers shown by VCSEL at frequencies (a) 1550 nm, (b) 1555 nm, (c) 1560 nm, and (d) 1565 nm.

in analysis of power driven by the system. The eye diagram shown in Figure 13 represents that noise, inter symbol interference, and jitter are almost nil in the communication channel using multiplexing with OAM waves.

The bit error rate is nil (Figure 13(b)) and shows good signal to noise ratio. Small dispersion can be seen in the output of multiplexed signal (Figure 14). The distortion is less; there is good S/N ratio at the sampling points (Figure 13(b)). The open eye area Figure 13(a) shows the best S/N ratio achieved. Earlier done experiments were 80/160 Tbit/s capacity achieved using 1600 nm wavelength with 16 QAM data channel with 80 wavelengths and two polarizations [64].

Experimentally pure OAM waves are generated using VCSEL at low cost with high efficiency SLM. The results were obtained for superposition of waves OAM for efficient topological charge. Relative phase of OAM can be turned from 0 to 2π, and the corresponding fringe patterns are achieved. These experiments are simulated using RSoft OptSim tool.

5.4. Demultiplexed Signal. Detected power [11] at the demultiplexer is represented mathematically as

$$\left[\psi_t{}'^{(\rho_0,\varnothing)}\right]^2 \cong \mathrm{DC}+\gamma_1 \cos\left(\varnothing+\Delta x_1\right)+\gamma_2 \cos\left(2\varnothing+\Delta x_2\right)+, \tag{50}$$

where DC is constant offset. γ are the coefficient of the Fourier series of azimuthally varying intensity patterns, and Δx_1 and Δx_2 are arbitrary constants. When an inverse operation is to be performed, spiral phase mask $\exp[-im\phi]$ can be used to remove the azimuthal phase dependence of an OAM beam.

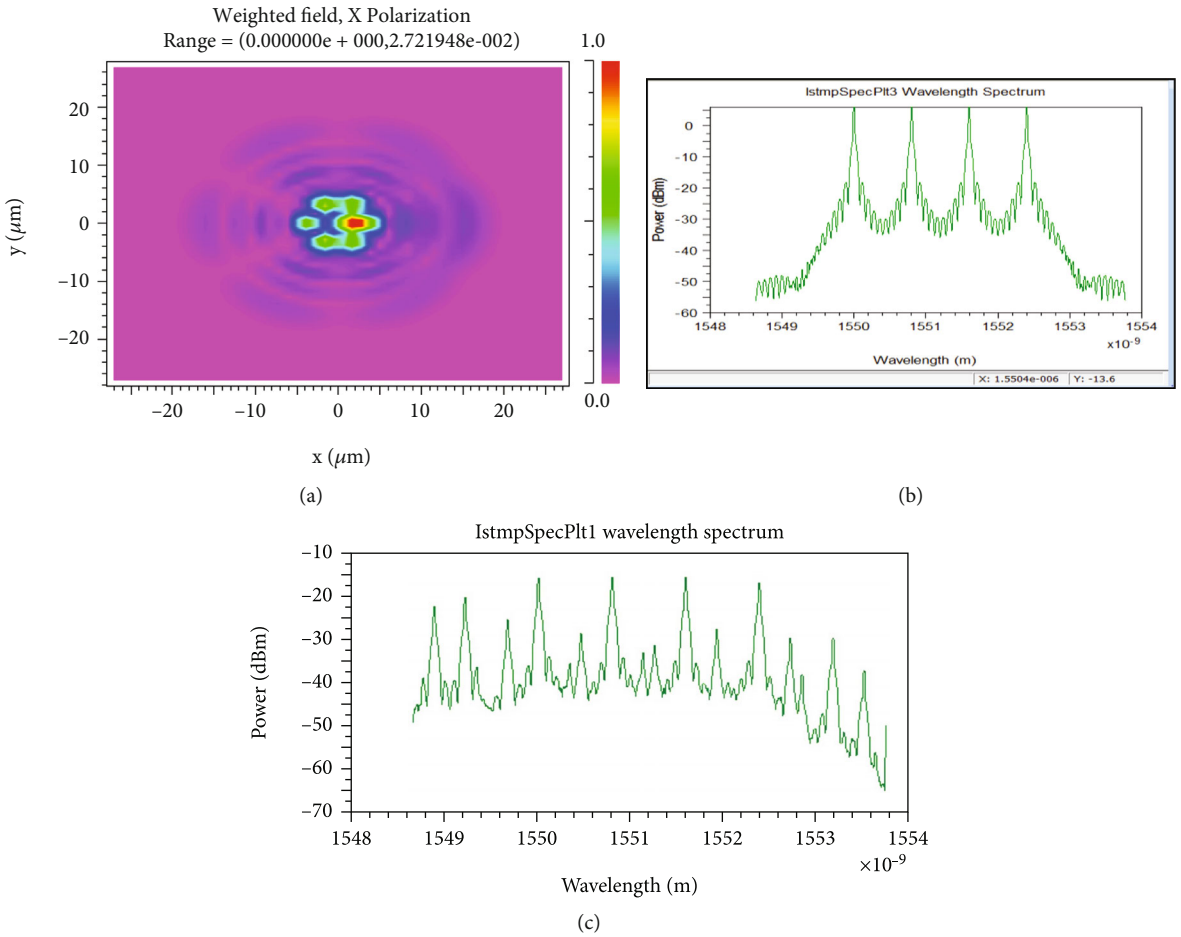

Figure 10: (a) Cross-sectional view of fiber carrying multiplexed output of 4 OAM waves using VCSELs, (b) multiplexed output of 4 OAM waves using VCSELs, and (c) multiplexed output of higher-number OAM waves using VCSELs.

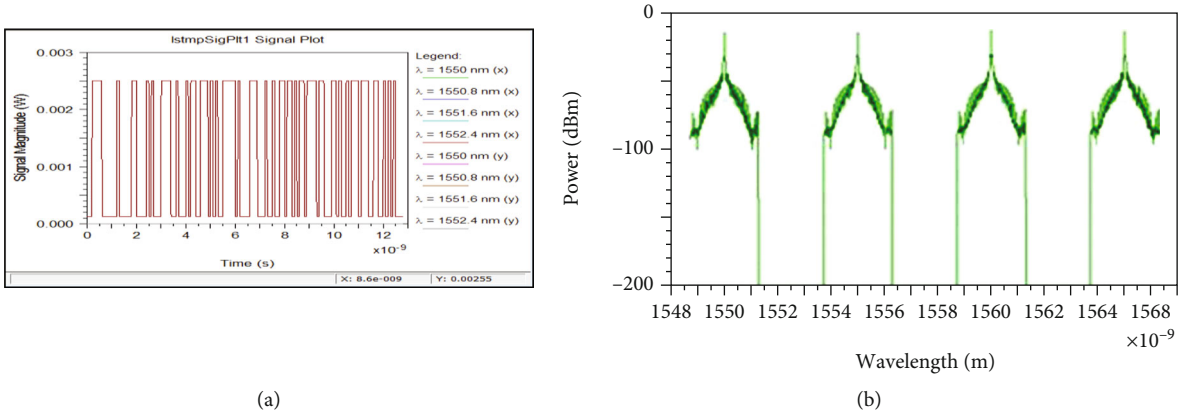

Figure 11: (a) Signal magnitudes of different wavelengths. (b) Power in dBm of multiplexed signals of different OAM generated as shown in Figures 9(a)–9(d) by four wavelengths.

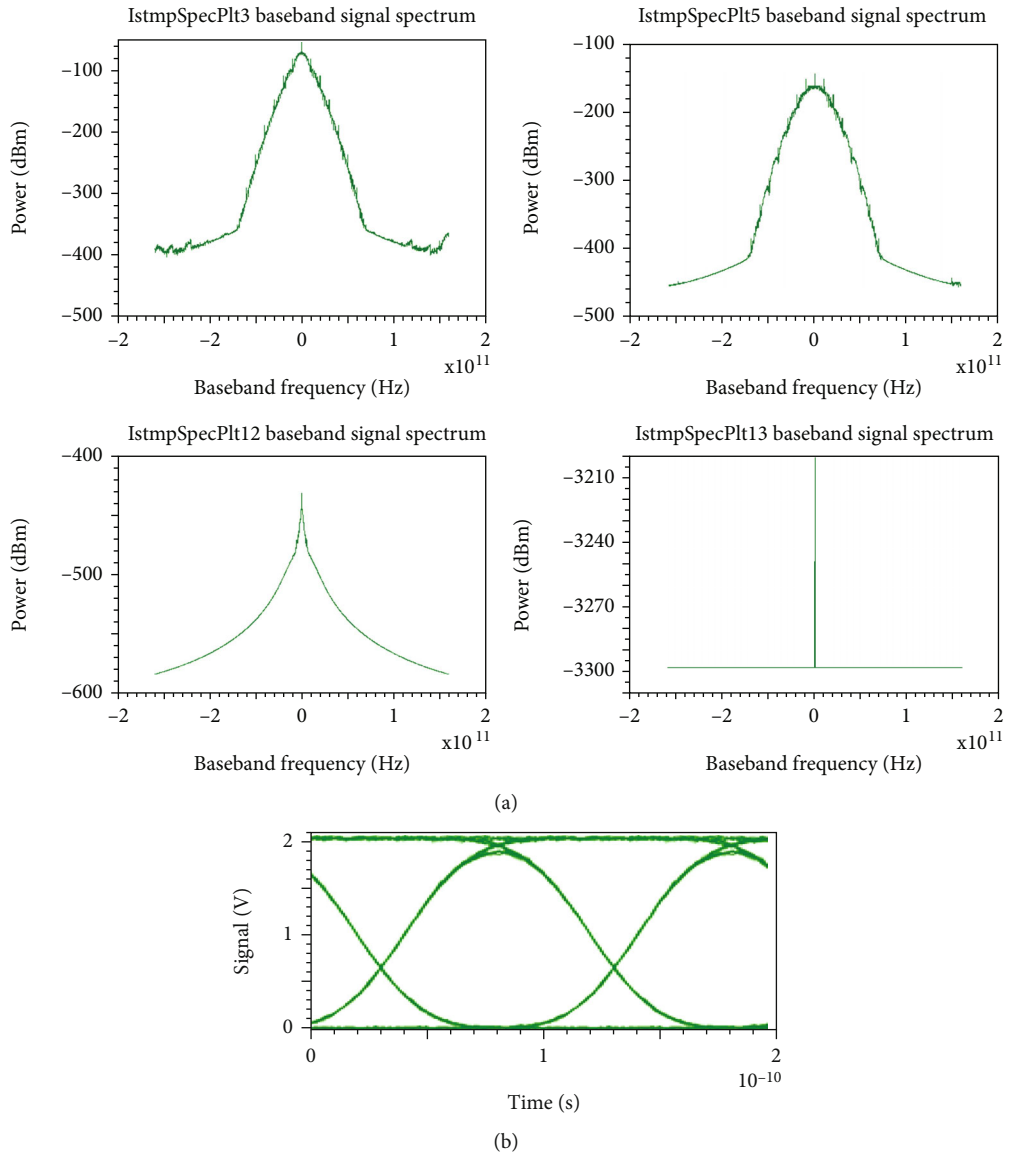

FIGURE 12: (a) Power spectrum achieved of four-baseband frequencies (Hz) in dBm by four wavelengths; (b) combined output of multiplexed signal eye diagram.

$$\psi_{\text{demux}}(\rho,\varnothing,t) = \exp\left[i(-l_{n'})\varnothing\right]\sum_{n=1}^{N}\psi_n(t)\psi_n{}^{\rho_x}(\rho).\exp\left(i.l_n.\varnothing\right),$$
$$= \psi_{n1}(t).\psi_{n1}{}^{\rho_x}(t) + \sum_{n=1,n1\neq n}\psi_n(t).\psi_n{}^{\rho_x}(r)\exp\left(l'_n\varnothing\right),$$
$$l'_n = l_n - l_q. \tag{51}$$

l_n, l_q are the n^{th} and q^{th} azimuthal number. Only one OAM beam is converted back to beam with the phase removed. All other waves remain the same. In practical applications, this beam is passed through a spherical lens to get back original beam.

Using a demuxing toolbox and a spatial analyzer (Figure 15), the demuxed output is obtained. The spatial modes are separated as shown in Figure 15.

Figure 15 shows demultiplexed signals having ring-shaped intensity profiles. Intensity is low at the center and radii proportional to the azimuthal index. This output shows OAM beams of 4 OAM channel after demultiplexing. The ring-shaped beam is converted into bright light intensity spots. These are coupled to optical fibers for detection [64].

6. Comparison with the Earlier Experiments

Earlier experiments done for 6 OAM modes for capacity of [36], 6 Tb/s over 119 km [64]. It gives high capacity [31, 32] in free space. Fiber-based OAM is also proven for 1.1 km high

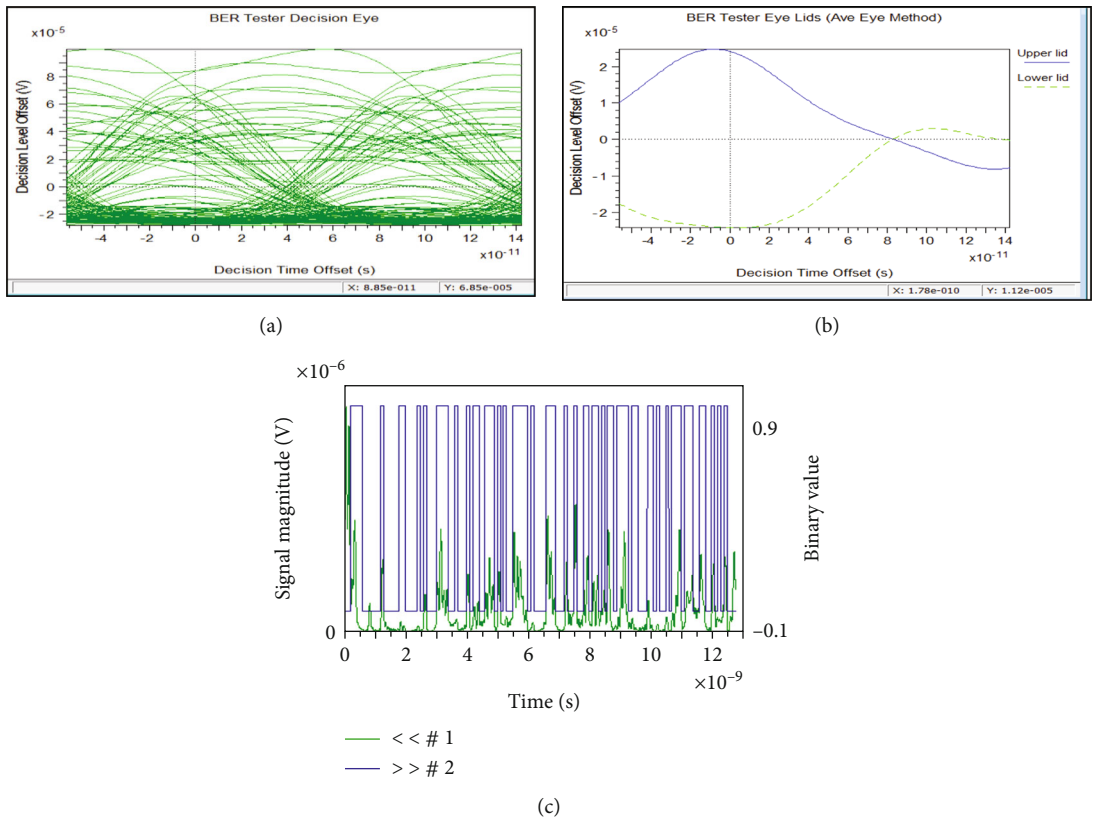

Figure 13: (a, b) Eye diagram multiplexed OAM waves with low bit error rate; (c) bit error signal magnitude in binary values.

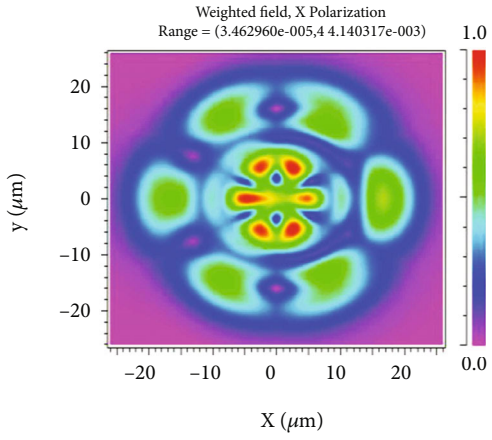

Figure 14: Output OAM multiplexed wave with dispersion.

capacity 1 Tb/s [36]. Orbital angular momentum multiplexing/demultiplexing [2] studies have been done. OAM beams are employed to encode information onto a laser beam for transmitting not only in fiber but also in free space communication [23, 46]. This also increases security in the link [23, 46]. The next-generation FSO will be achieved by OAM. This research focuses on the quantum and classical aspects. This research brings overall methodologies and discussions on OAM using mathematical derivations of all the OAM waves and its experimental validation for LG waves using VCSELs with the help of simulations. Some of the derivations will be analyzed using quantum mechanics in the near future.

The two OOK signal modulations of 1.5 Gb/s were directly modulated with 445 nm laser diode. These channels were carried by two OAM modes used for underwater optical communication [21]. The results with lowest cross-talk have been proved with optical [21] vortices of Si waveguides. Several methods have been shown by earlier work. We can generate OAM by diffraction grating. Beams and incident coaxial optical vertices beam carrying massive OAM and demultiplexing using single Dammann optical vortex gratings (DOVGs), by [21] topological charge equal to zero. From one DOVG, several OAM can be generated and similarly be detected using sufficient diffraction angle interval to arrange appropriate filters and detectors.

6.1. Comparison of Methods with Previous Known Methods. PCBs and printed circuit boards are used [54]. Other techniques are antenna arrays, holographic plates, and inhomogeneous birefringent devices for generating OAM beam. One experiment [54] for multiplexing OAM was proposed designing a nonpolarizing beam splitter where 4 OAMs are generated by 4 SPPs and using nonpolarizing beam splitter; multiplexing was done. Similarly, antenna array is used to generate intermodulated OAM modes. Other low-cost OAM generation is by using different holes on a planar antenna substrate in PCB technology [34, 54]. Metasurfaces generate dual modes with polarization-dependent transmission and reflection properties.

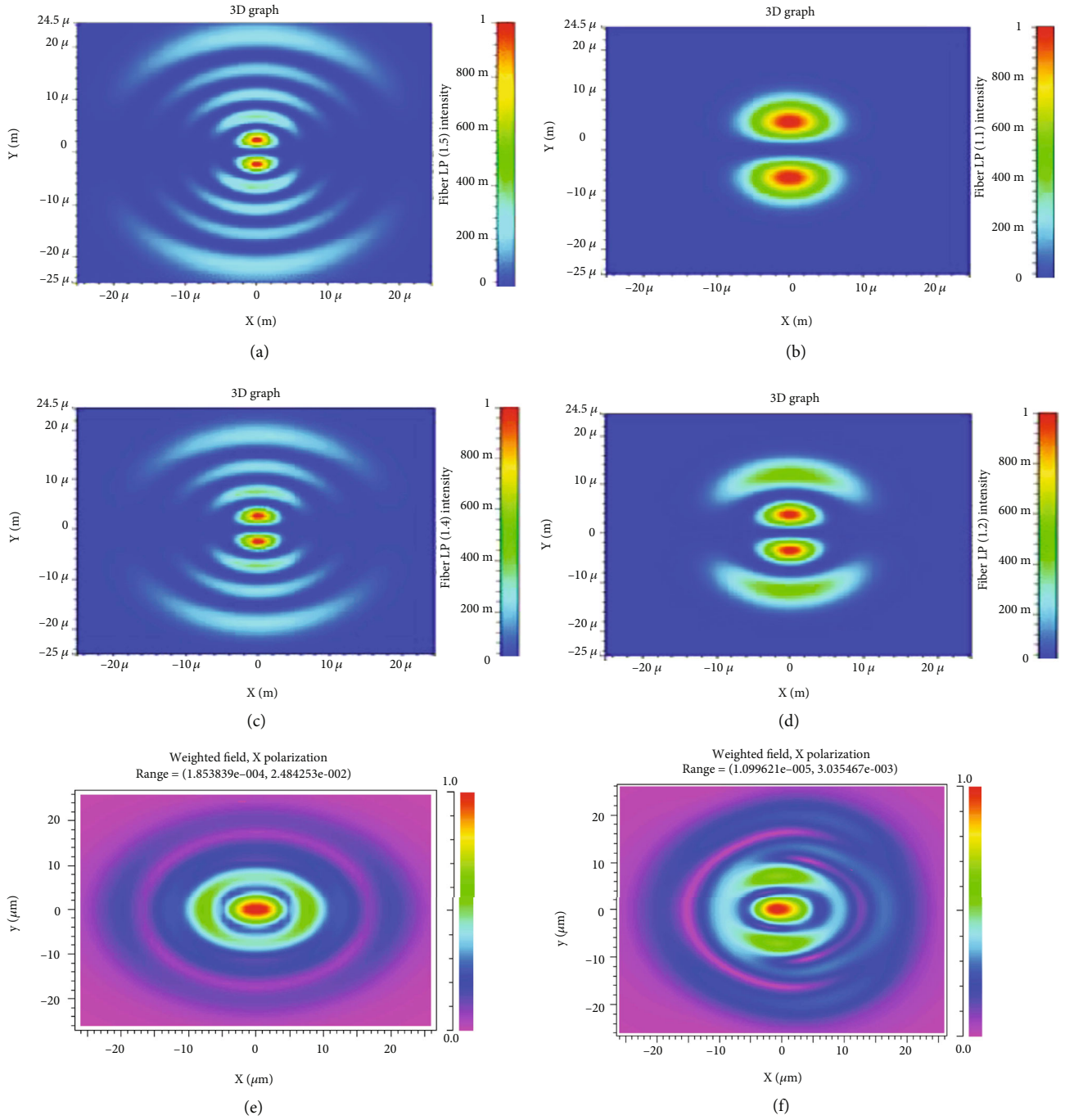

FIGURE 15: Demultiplexed output OAM waves. Demultiplexed signals are achieved for $m = 4$, $n = 1$; $m = 0$, $n = 1$; $m = 3$, $n = 1$; $m = 1$, $n = 1$.

These muxed waves are the key to QKD Quantum Key Distribution protocols when we superimpose $[+1>,|-2>]$, $[+1> +-$ quantum optics [38] two-dimensional QKD for higher dimension quantum optics.

Spatial high modulation is limited to a millisecond response time. Greater conversion efficiency is achieved through SPP based spiral phase plates. SLM has no possibility of miniaturization and integrated components. The innovation research on OAM by Willner et al. [21] shows exactly the given solution of the research and proves the results obtained in Figures 8–Figure 13 discussed mathematically in this paper.

Li et al. demonstrated a 64 Gbps [34] FSO link using PAM-4 modulations experimented using VCSEL for 88 Gbps data transmission over 555 m free-space length. It uses WDM and PAM-4 techniques [27]. SPP (spiral phase plates) used to give OAM waves giving an angle of $2\pi l$ phase shift over the full circle when incident EM wave falls upon SPP wave.

Hardware [34] is used for the OAM generation. The intensity profiles we get are using RSoft analyzers. In addition to this, RSoft-simulated work validates the multiplexing of signals. These signals are good especially for short-reach data interconnection and QKD. In this experiment, Gaussian beam

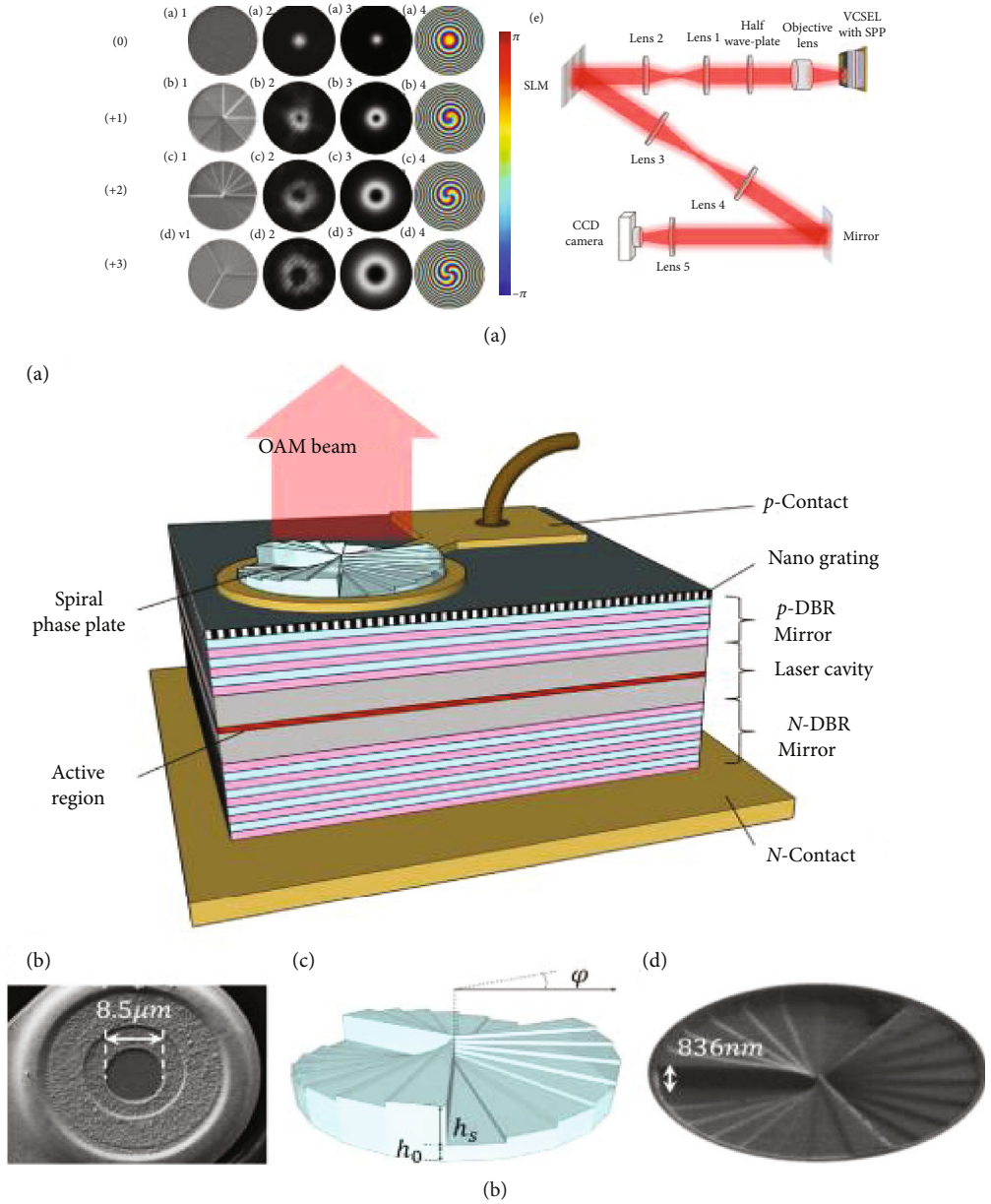

Figure 16: (a) Experimental setup of OAM generation by VCSEL [Figure 2, [68]]. (b) SPP plate [Figure 1, [68]].

is sent to laser and we get OAM waves at the outputs. We use spiral phase plates to generate different intensity profiles of OAM as shown in Figure 16.

Experiments also show the superimposed beams of OAM [34]. It also shows diffraction in the multiplexed output beams. Figure 17(e) shows the superimposition of waves *a*, *b*, and *c*, which shows the intensity profile of the OAM waves. Figure 17(e) shows the diffraction in the multiplexed beams. OAM beams are generated by cylindrical lenses, spherical plates, and diffractive optics. The number of channels in OAM is an important property. Some of the techniques are photonic crystal fiber, with spiral PCF; hence, circular PCF has been designed at [54] 1000 nm wavelength.

Inverse phase hologram is used to recover data on one of the OAM beams [54].

Another approach that gained much attention is to transmit independent data, each in a different core using multicore fibers (MCF) [11, 67]. By increasing the number of spatial modes, fiber capacity and the spectral efficiency of the channel increases.

7. Discussions

In this research, classical and quantum behaviors of OAM waves were analyzed. It proves a successful implementation of wired photonic circuit using VCSEL for a single wavelength and multiple wavelength OAM generation and multiplexing/demultiplexing using OAM. It is observed that OAM waves are not distorted when demultiplexed. It proves

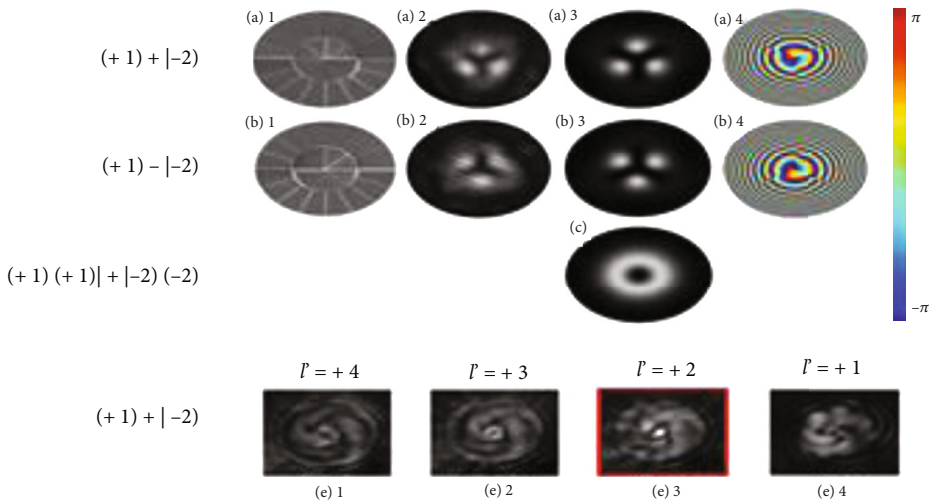

Figure 17: Superposition of waves generated by SPP and diffraction in the mixed output [Figure 3, [68]].

that OAM requires very low power in milliwatt range in multiplexing and demultiplexing.

Multiplexing in OAM modes and higher order LP modes are composed [55] of $LP_{21} = HE_{3,1} + EH_{1,1}$, two eigenmodes $OAM_{0,2} = HE_{2,1}{}^{even} + i \times HE_{2,1}{}^{odd}$. OAM is combined by two fiber eigenmodes. They have the same propagation constant as compared to LP mode components of different propagation constants; OAM mode components of same propagation constants will not suffer from intrinsic mode walk off. So OAM gives a stable propagation through a certain length of fiber. Single-ring fiber [43] of high index maintains radially fundamental modes and reduces cross-talk during mode excitement. To increase the number of eigenmode coupling through the fiber, either the core radius is increased [43] or the RI difference between core and cladding is increased.

Single fiber gives 1-D MDM. By using multiple ring fiber interring cross-talk [61] can be minimized, OAM modes with different phases into high-index ring regions are multiplexed in spatial dimensions.

OAM beams are used for free space and fiber-based communication links. Multiple OAM beams each having a unique twisting value carries an independent data stream which are multiplexed at the transmitter. At the receiver side, these OAM modes are demultiplexed and the resultant Gaussian beam is propagated through a single mode fiber for data recovery. 16 QAM data capacity of 1.4Terabit/sec additionally 100 Tb/s free-space data link was reported by simultaneously combining/multiplexing OAM. QPSK signal of 1008 channels was successfully tested [61] with a capacity 100.8Tbot/s.

7.1. Further Advancement and Connected Technologies. OAM can be categorized as OAM–SK and OAM–DM (shift keying and division multiplexing). It has increased the data rate from terabit to petabit [64]. 100 Tbit/s data capacity achieved through multiplexing of 42 wavelengths, 120 AM beams, and two polarization states.

For demultiplexing and detection mechanism, optical vortex grating is used for the multiplexing of OAM channels with individual modulation schemes and simultaneous detection mechanisms [64]. Four-level PAM for FSO link of [24] 16000Gbps input streams is successfully implemented with OAM having low BER value $\sim 10^{-9}$ with clear eye diagrams. QPSK inputs with SMM/SMD in MIMO lusing [23]1550 nm wavelength OAM modes are proves to give turbulent-free FSO. OAM-based MIMO systems are the next coming technology which has greater channel capacity [64] than conventional MIMO systems.

8. Applications of OAM

OAM finds applications in wired and wireless communication technologies. For wired technologies, encoding with OAM is done. Assuming a network of users transmitting photonic qubits, data encoding is done with three degree of freedom-path, polarization, and OAM. Photon degrees of freedom is used in terms of polarization, time, frequency, phase, and OAM. This gives different quantum communication protocols. If OAM is used for multiplexing under atmospheric turbulences, it provides higher security in terms of total secrecy. OAM can be controlled by controlling Q factor of cavity. This opens a door towards the next-generation molecular sciences and applications.

Optical vortices have advanced applications as optical tweezers. Quantum mechanics is used in high order quantum entanglement, nonlinear optics, and classical models of optical vortices.

In free space communication (FSO), the FSO receiver link [8, 38] is designed based on the orthogonality of the Laguerre–Gaussian (LG) beams with different azimuthal mode numbers. Transmitters and receiver links are designed. This enables ultra-high-speed transmission to end-users, allowing interoperability of various RF and optical technologies. It increases the BER performance of the modulation and reduces the complexity of receivers. FSO is being used in UWB communication, in satellite communication, deep space communication, satellite to aircraft communication, and aircraft to satellite communication. In all the cases, atmospheric turbulence does not affect the communication. This technology will meet the

high demand of increasing bandwidth and channel capacities in today's world.

9. Conclusion

OAM has tremendous ability to increase the capacity of channels in terms of data in the terabit transmission. Optical communication having larger bandwidth increases the data spectral efficiency by using polarization, amplitude, and phase of the optical signal.

For this, SDM, WDM, MDM are to be used, which gives scope for optical communication in terms of low attenuation of signals, better bit error rate, low interchannel interference, and less cross-talk, leaving behind copper communication. The system performance can be improved by the Laguerre–Gaussian vortex, hypergeometric beams, and combined Gaussian-vortex beams. Thus, OAM beams in today's network provide an essential aid for free space communication, underwater optical communication, satellite communication, and sensing systems. The OAM waves received after scattering from target give information of azimuth hence, finds tremendous scope in target detection. In future, only optical communication has the ability to provide large capacity high-speed communication which can meet the demand of network broadband services and scientific communities. It will be further expanded in fiber communication using quantum optics for QKD and higher security channel designs.

9.1. Future Scope. These advantages with OAM waves assure that in the near future, quantum technologies will dominate the traditional communication techniques because of very low power consumption and ease of generating these modes. This also opens an area for quantum computing and quantum cryptography. Future work lies on metasurfaces, where by controlling the polarization, we can achieve these optical transmitters and receivers in compact designs.

Appendix

A. A.1

EM wave has angular momentum component is in the z direction. A component of linear momentum is in the x, y plane. Linear momentum density is given by

$$p = \epsilon_0 E \times B, \tag{A.1}$$

and angular momentum density

$$L = r \times p. \tag{A.2}$$

ϵ_0 is the dielectric permittivity of the fiber; E and B are electric and magnetic fields.

Here, $E = i\hbar(\partial/\partial t)$.

B. A.2

Here, the photon is in the eigenstate along the z axis defined by angular momentum operates l_z in classical theory as

$$l_z = (h/i)\,(\partial/\partial \varnothing)(\text{in cylindrical coordinate}).$$
$$v_{nm}(\rho,\varnothing,z) = x_{nm}(\rho, z)e^{\text{in}\varnothing}. \tag{B.1}$$

C. A.3

In terms of components, L_x, L_y, and L_z are, respectively, the three Cartesian components of the angular momentum operator in quantum mechanics. They also represent the generators of rotations around the three axes in the representation L^2 (R). In a representation of the rotation group where the squared total angular momentum operator has eigenvalue $l(l+1)$,L_x, L_y and L_z have eigenvalues $-l, -l+1, \cdots, l-1, l$. In particular, if the representation is $l = 1$, L_x, L_y, and L_z have eigenvalues of 1, 0, and -1. Polarized light can be either left circularly polarized, right circularly polarized, or a linear combination of these two states. Thus, polarized light has eigenvalues +1 or -1 for any component of the angular momentum. The 0 eigenvalue does not occur. We thus say that the photon is a spin one particle. If we wish to describe waves produced by other particles having, say, spin m, then we must use the other representations of the rotation group, i.e., for $m = 2, 3, \cdots$, in the case of Boson's and half integers I the case of fermions.

D. A.4

LP modes in $(\rho,\varnothing, z)$ defines the cylindrical waveguide, and classical wave is represented in this form. It can also be represented as a quantum wave in azimuthal and spin angular momentum operator n, m where $\varnothing$ is the azimuthal angle.

E. A.5

In the quantum theory of electromagnetic fields, moment of vector potential $A(\rho, t)$ which satisfies the homogeneous wave equations, where its spatial solutions are given by exp $(i.k.\rho)$ [15]. Specifying a volume of a cavity length L [38] with electromagnetic wave travelling inside the cavity assuming a vector potential [38] $A(\rho, t) = A_0\, v(\rho, t)\hat{n}$. Here, $\hat{n}$ is a unit vector, and $A(\rho, t)$ is specifying product of temporal and spatial part.

Electric field and magnetic field in the cavity in terms of scalar wave potential A are

$$E = \frac{-1}{c}\,\frac{\partial A}{\partial t} \text{ and } B = \nabla \times A, \tag{E.1}$$

From curl of vector A,

$$\nabla \times \nabla \times \nabla = \nabla(\nabla.\mathrm{A}) - \nabla^2 \mathrm{A},$$
$$\left(c^2k^2 + \frac{\partial^2}{\partial t^2}\right)A(\rho, t) = 0, \tag{E.2}$$
$$\left[\mathrm{c} = \left(\frac{1}{\mu_0 \epsilon_0}\right)^{-1/2}\right].$$

The vector potential:

$$A(t) = A_0 u(\rho) e^{-ik.\rho.t}. \tag{E.3}$$

This is the solution of spatial part.

Temporal part solution is exp $(\mp i\omega_k t)$.

From Maxwell's equations $\omega_k = c\,\mathrm{k}$, with $k \equiv |k|$. Assuming field

$$\Psi(\rho, t) = \Psi(\rho) e^{-ikct}. \tag{E.4}$$

F. A.6

OAM waves can also be represented by [42] vector potential as

$$\varphi(x) = A(x)\, e^{i\varnothing\rho}, \tag{F.1}$$

where

$$\varphi(x) = \pm\frac{1}{h}\int p(x)dx,$$
$$\varphi(x) \cong \frac{c}{\sqrt{p(x)}}\, e^{\pm 1/h \int p(x)dx}. \tag{F.2}$$

$|x|^2 \cong |c|^2/p(x)$ is defined as probability of finding the particle at point x from 0 to r which is inversely proportional to its classical momentum given by [41]

$$\int_0^r p(x)dx = n'\pi h, \tag{F.3}$$

and $\varnothing(\rho) = n'\pi$.

The energy of particle in OAM is $E_{n'} = n^2\pi^2h^2/2m\rho^2$.

G. A.7

$u(r) = u(\rho,\varnothing,z)$ is a basis defined in $V_{nm}(\rho,\varnothing,z) \approx V_{nm}$

Eigenvalues are

$$=> l_z v_{mn}(\rho,\varnothing,z) = \frac{\hbar}{i} x_{mn}(\rho, z)\frac{\partial}{\partial\varnothing} e^{\mathrm{in}\varnothing},$$
$$= n\hbar v_{mn}(\rho,\varnothing,z). \tag{G.1}$$

Azimuthal phase dependence is $e^{im\varnothing}$.

Vector potential is finally expressed as

$$A|\rho, t> = A_0 \sum_{mn} C_{mn} x_{nm}(\rho, z) e^{-ikct+im\varnothing}, \tag{G.2}$$

where $\sum_{mn}|C_{mn}|^2 = 1$ using quantum mechanics

$$v_{nm} \longrightarrow |m, n> = \gg,$$
$$l_z|m, n> n'\hbar|m, n>. \tag{G.3}$$

These eigenstates are normalized with the following conditions [2, 41]:

$$<m, n|m', n'> = \iint_{R^2} v_{mn}(x, y, z) v_{mn}(x, y, z)dxdy = \delta mm'\, \delta nn' \tag{G.4}$$

an observable A represented in this basis as

$$<m, n|A|m', n'> = A_{mm'nn'}$$
$$\left|M> = \sum_{h=-\infty}^{\infty}\sum_{m=0}^{m=\infty} C\,mn\right|m', n'>. \tag{G.5}$$

$|M>$ is the photon state.

Increasing or decreasing the radial number by one unit, with l unchanged creates (anhiliate) one positive quantum and one negative quantum number. "n" is the quantum number [67] because of degeneracy in m.

H. A.8

The following shows the transmission of LP modes in optical fiber:

The spatial modes travel in the form of linearly polarized modes in the fiber.

If linear moments are given by [41] $p_x = -i\hbar(\partial/\partial x)$, $p_y = -i\hbar(\partial/\partial y)$, $p_z = -i\hbar(\partial/\partial z)$.

Optical fiber wave equation is given by $E\psi = (1/2m)(p_x{}^2 + p_y{}^2 + p_z{}^2)\psi = (p^2/2m)\psi$

The vector quantities p (p=px, py, pz)

Expression gives the LG modes. J_x, J_y, J_z defined in terms of p_x, p_y, p_z give solution to the LP modes. The electrons are distributed in a spiral along the beam axis, which gives a helical density modulation. Bunching factor is given by integrating over the $dz\,d\phi$ where $f(z, \phi)$ the normalized distribution of the trapped electron is, k is wave number and l is azimuthal mode index.

$$b_1(k) = \left|\int dz\, d\phi f(z, \phi)\, \exp\,(ikz + il\phi)\right|. \tag{H.1}$$

The combined form of OAM wave is given by

$$E = E_x e^{i\,(kz-\omega t+\delta)} e_x + E_y e^{i\,(kz-\omega t+\delta)} e_y, \tag{H.2}$$

e_x, e_y are two rectilinear polarizations with respect to k

propagation wave vector. OAM modes [11] generated in the fibers or the cylindrical waveguide are represented as a complete basis of LG mode represented by

$$V_{nm} = \frac{e^{in\phi}}{d(z)}\sqrt{\frac{2m!}{\pi\,(m+|n|)!}}\left(\frac{\rho\sqrt{2}}{d(z)}\right)^{|n|} \times L_m^{|n|}\left(\frac{2\rho^2}{d(z)^2}\right).\exp\left(-\left(\frac{\rho}{d(z)}\right)^2 - \frac{ik_0\rho^2 z}{2\left(z^2+z_\rho^2\right)}\right),$$
$$\times \exp\left[\left(i(2m+(|n|+1))\arctan\frac{z}{z_\rho}\right)\right],$$
$$\text{with } \rho = \sqrt{x^2+y^2} \text{ radius,} \tag{H.3}$$

and $\theta = \arctan\ (y/x)$, $\exp\left[(i(2m+(|n|+1))\arctan(z/z_\rho)\right)$.

It is defined as Gouy phase.

$$d = d(0)\sqrt{\frac{\left(z^2+z_\rho^2\right)}{{z_\rho}^2}} \text{ is beam radius.} \tag{H.4}$$

z_ρ is the Rayleigh range of beam, [46] is the beam waist, and $L_m^{|n|}(:.)$ are the associated Laguerre Polynomials with $m \in N$ and $n \in \mathbb{Z}$[47].n is the azimuthal index giving of $l\hbar$ per photons, and m is number of radial nodes in the intensity distribution. For $l > 0$ LG modes comprise $m+1$ concentric rings with zero on axis intensity.

Laguerre polynomial is given by [6].

$$L_m^{|n|}(x) = (-L)^{|n|}\frac{d^{|n|}}{d_x{}^{|n|}}L_{n+|l|}(x). \tag{H.5}$$

l is defined as azimuthal index of OAM given by $l\hbar$ per photon, and n is the number of radial nodes for $l > 0$.

In defining $L_m^{|n|}$ as generalized Laguerre Polynomials,

$$\tilde{m} = \frac{\left(n' - |n|\right)}{2}. \tag{H.6}$$

Probability distribution $|P_{nl}(\mathrm{r},\varphi)|^2$ shows m dark concentric rings.

$$\tilde{m} \longrightarrow \frac{1}{2}\left(n' - l\right) = \begin{cases} n'_-, & \text{for } l > 0, \\ n'_+, & \text{for } l > 0. \end{cases} \tag{H.7}$$

It is a radial number operator of the Laguerre Gaussian mode.

Abbreviations

MIMO: Multiple Input and Multiple Output
OAM: Orbital angular momentum
SDM: Spatial domain multiplexing
VCSELs: Vertical cavity surface emitting lasers
WDM: Wavelength division multiplexing
FSO: Free space communication
OAMBS: OAM Beam Splitter
SAM: Spin angular momentum
UWB: Ultrawideband
RSOFT: RSOFT photonic device tool OptSim used for simulation
OV: Optical vertices
HGM: Hypergeometric beams
MMF: Multimode fiber
SLMs: Spatial light modulators
LG: Laguerre–Gaussian
HG: Hypergeometric
HGM: Hermite–Gaussian
SLM: Spatial light modulators
UOC: Underwater optical communication
OAM–SK: OAM shift keying
OAM–DM: OAM division multiplexing
PCF: Photonic crystal fibers
UAV: Unmanned aerial vehicles RCF (ring core fiber)
LHCP: Left hand circularly polarized
RHCP: Right hand circularly polarized
HGG: Geometric Gaussian
QAM: Quadrature amplitude modulation
DOVG: Dammann optical vortex gratings
RI: Refractive index
ERI: Effective refractive index
NA: Numerical aperture
SMM/SMD: Spatial multimode multiplexing/spatial mode multiplexing
FSO: Free Space Optics
PAM: Pulse amplitude modulation
QPSK: Quadrature phase shift keying QKD -Quantum Key Distribution

Data Availability

All the data presented has been presented in the paper, and other data required are available upon request.

Ethical Approval

This manuscript is not based on data of human tissues or studies on the data of animals.

Conflicts of Interest

There is no conflict of interest. This study was completed as part of employment in the Department of Electronics and Communication Engineering Netaji Subhash University of Technology East Campus Delhi.

Acknowledgments

The authors are thankful to the Department of Electronics and Communication NSUT East Campus for extending help in optical communication laboratories to complete the research.

References

[1] L. Gong, Q. Zhao, H. Zhang et al., "Optical orbital-angular-momentum-multiplexed data transmission under high scattering," *Light: Science & Applications*, vol. 8, no. 1, p. 27, 2019.

[2] A. E. Willner, H. Huang, Y. Yan et al., "Optical communications using orbital angular momentum beams," *Advances in Optics and Photonics*, vol. 7, no. 1, pp. 66–106, 2015.

[3] N. Bozinovic, Y. Yue, Y. Ren et al., "Terabit-scale orbital angular momentum mode division multiplexing in fibers," *Science*, vol. 340, no. 6140, pp. 1545–1548, 2013.

[4] J. Wang, S. Li, C. Li et al., "Ultra-high 230-bit/s/Hz spectral efficiency using OFDM/OQAM 64-QAM signals over polmuxed 22 orbital angular momentum (OAM) modes," in *Optical Fiber Communication Conference*, pp. W1H–W14, San Francisco, USA, 2014.

[5] A. E. Willner, H. Huang, Y. Yan et al., "Optical communication using multiplexing of multiple orbital angular momentum beams," *Advances in optics and photonics*, vol. 7, no. 1, pp. 66–106, 2015.

[6] J. Wang, J. Y. Yang, I. M. Fazal et al., "Terabit free-space data transmission employing orbital angular momentum multiplexing," *Nature Photonics*, vol. 6, no. 7, pp. 488–496, 2012.

[7] L. Allen, M. W. Beijersbergen, R. J. Spreeuw, and J. P. Woerdman, "Orbital angular momentum of light and the transformation of Laguerre-Gaussian laser modes," *Physical review A*, vol. 45, no. 11, p. 8185, 1992.

[8] J. Wang, "Advances in communications using optical vortices," *Photonics Research*, vol. 4, no. 5, pp. B-14–BBZ8, 2016.

[9] M. Padgett and R. Bourman, "Tweezers with a twist," *Nature Photonics*, vol. 5, no. 6, pp. 343–348, 2011.

[10] S. Ramachandran and P. Kristenreen, "Optical vortices in fiber," *Nanophotonics*, vol. 2, no. 5-6, pp. 455–474, 2013.

[11] A. M. Yao and M. J. Padgett, "Orbital angular momentum: origins, behavior and applications," *Advances in Optics and Photonics*, vol. 3, no. 2, pp. 161–204, 2011.

[12] S. H. Mushid, S. Alanzi, and B. Chowdhury, "Method and applications for multiplexed optical communication system using spatial domain multiplexing (SDM) and orbital angular momentum of photon (OAM) multiplexing with wavelength division multiplexing (WDM)," U.S. Patent No. 9,712,239 2017.

[13] S. Chen, B. Yang, Y. He et al., "Optical orbital angular momentum shift-keying communication based on coherent demodulation," *Optics Communications*, vol. 452, pp. 405–410, 2019.

[14] X. I. Wang, X. D. Cai, Z. E. Su et al., "Quantum teleportation of multiple degrees of freedom of a single photon," *Nature*, vol. 518, no. 7540, pp. 516–519, 2015.

[15] Z. Tagay and C. Valagiannopoulos, "Highly selective transmission and absorption from metasurfaces of periodically corrugated cylindrical particles," *Physical Review B*, vol. 98, no. 11, article 115306, 2018.

[16] Z. H. Fang, H. Chen, D. An, C. R. Luo, and X. P. Zhao, "Manipulation of visible-light polarization with dendritic cell-cluster metasurfaces," *Scientific Reports*, vol. 8, no. 1, p. 9696, 2018.

[17] X. Chen, Y. Zhou, X. Ma, W. Fang, W. Zhang, and W. Gao, "Polarization conversion in anisotropic dielectric metasurfaces originating from bound states in the continuum," *Optics Letters*, vol. 46, no. 17, pp. 4120–4123, 2021.

[18] C. A. Valagiannopoulos, M. Mattheakis, N. S. Shirodkar, and E. Kaxiras, "Manipulating polarized light with a planar slab of black phosphorus," *Journal of Physics Communications*, vol. 1, no. 4, article 045003, 2017.

[19] A. Sarsen and C. Valagiannopoulos, "Robust polarization twist by pairs of multilayers with tilted optical axes," *Physical Review B*, vol. 99, no. 11, article 115304, 2019.

[20] S. Yu, "Potentials and challenges of using orbital angular momentum communications in optical interconnects," *Optics Express*, vol. 23, no. 3, pp. 3075–3087, 2015.

[21] A. E. Willner, K. Pang, H. Song, K. Zou, and H. Zhou, "Orbital angular momentum of light for communications," *Applied Physics Reviews*, vol. 8, no. 4, article 041312, 2021.

[22] J. Wang, J. Liu, S. Li, Y. Zhao, and L. Zhu, "Orbital angular momentum and beyond in free-space optical communications," *Nonophotonics*, vol. 11, no. 4, pp. 645–680, 2022.

[23] B. B. Yousif and E. E. Elsayed, "Performance enhancement of an orbital-angular-momentum-multiplexed free-space optical link under atmospheric turbulence effects using spatial-mode multiplexing and hybrid diversity based on adaptive MIMO equalization," *IEEE access*, vol. 7, pp. 84401–84412, 2019.

[24] B. Dutta, N. Sarkar, R. Atta, B. Kuiri, and A. S. Patra, "1600 Gbps PAM-4 FSO link enabled using OFCL-based WDM and OAM-multiplexing techniques," *Results in Optics*, vol. 9, article 100287, 2022.

[25] B. B. Yousif, E. E. Elsayed, and M. M. Alzalabani, "Atmospheric turbulence mitigation using spatial mode multiplexing and modified pulse position modulation in hybrid RF/FSO orbital-angular-momentum multiplexed based on MIMO wireless communications system," *Optics Communications*, vol. 436, no. 1, pp. 197–208, 2019.

[26] L. Li, R. Zhang, Z. Zhao et al., "High-capacity free-space optical communications between a ground transmitter and a ground receiver via a UAV using multiplexing of multiple orbital- angular-momentum beams," *Scientific Reports*, vol. 7, no. 1, 2017.

[27] K. Mukherjee, B. Mallick, S. Kuiri et al., "PAM-4 based long-range free-space-optics communication system with self injection locked QD-LD and RS codec," *Optics Communications*, vol. 476, article 126304, 2020.

[28] K. Liu, Y. Cheng, H. Wang, Y. Qin, and X. Li, "Orbital-angular-momentum-based electromagnetic vortex imaging," *IEEE Antenna and wireless propagation letters*, vol. 14, pp. 711–714, 2015.

[29] F. E. Mahmouli and S. Walker, "Orbital angular momentum generation in a 60GHz wireless radio channel," in *2012 20th Telecommunications Forum (TELFOR)*, pp. 315–318, Belgrade, Serbia, 2012 Nov 20.

[30] Y. Shen, X. Wang, Z. Xie et al., "Optical vortices 30 years on: OAM manipulation from topological charge to multiple singularities," *Light: Science & Applications*, vol. 8, no. 1, p. 90, 2019.

[31] X. Cai, J. Wang, M. J. Strain et al., "Integrated compact optical vortex beam emitters," *Science*, vol. 338, no. 6105, pp. 363–366, 2012.

[32] N. K. Fontaine, C. R. Doerr, and L. L. Buhl, "Efficient multiplexing and de multiplexing of free space orbital angular momentum using photonic integrated circuits," in *Optical Fiber Communication, Conference OSA*, Technical Digest optical society of America, 2012.

[33] A. Suprano, D. Zia, E. Polino et al., "Enhanced detection techniques of orbital angular momentum states in the classical and quantum regimes," *New Journal of Physics*, vol. 23, no. 7, article 073014, 2021.

[34] H. Li, D. B. Phillips, X. Wang et al., "Orbital angular momentum vertical-cavity surface-emitting lasers," *Optica*, vol. 2, no. 6, pp. 547–552, 2015.

[35] Y. Yan, G. Xie, H. Huang et al., "Demonstration of 8-mode 32-Gbit/s millimeter-wave free-space communication link using 4

orbital-angular-momentum modes on 2 polarizations," in *2014 IEEE International Conference on Communications (ICC)*, pp. 4850–4855, Sydney, NSW, Australia, 2014 Jun 10.

[36] T. Lei, M. Zhang, Y. Li et al., "Massive individual orbital angular momentum channels for multiplexing enabled by Dammann gratings," *Light Science & application*, vol. 4, no. 3, p. e257, 2015.

[37] S. Chen and J. Wang, "Theoretical analyses on orbital angular momentum modes in conventional graded-index multimode fibre," *Scientific Reports*, vol. 7, no. 1, 2017.

[38] A. K. Ghatak and S. Lokanathan, *Quantum Mechanics: Theory and Applications*, Macmillan, 2004.

[39] S. N. Khonina, V. V. Kotlyar, M. V. Shinkaryev, V. A. Soifer, and G. V. Uspleniev, "The phase rotor filter," *Journal of modern optics*, vol. 39, no. 5, pp. 1447–1454, 1992.

[40] G. Keiser, *Optical Communication*, vol. 2, Tata Mc Graw Hill, New York, 5th Edition edition, 2000.

[41] C. K. Huang, N. Lemos, X. Xu, and C. Joshi, "OAM in the light emitted from laser plasma acceleration," in *17th Advanced Accelerator Concepts Workshop*, National Harbor, MD, 2016.

[42] D. Petrosan and P. Lambropoulos, *Fundamental of Quantum Optics and Quantum Information*, Springer, 2007.

[43] S. C. Chu, Y. T. Chen, K. F. Tsai, and K. Otselka, "Generation of high-order Hermite-Gaussian modes in end-pumped solid-state lasers for square vortex array laser beam generation," *Optics Express*, vol. 20, no. 7, pp. 7128–7141, 2012.

[44] M. L. Chen, L. J. Jiang, and W. E. Sha, "Orbital angular momentum generation and detection by geometric-phase based metasurfaces," *Applied Sciences*, vol. 8, no. 3, p. 362, 2018.

[45] S. Dalgac and K. Elmabruk, "The Propagation of Vortex Beams in Random Mediums," in *Vortex Dynamics-From Physical to Mathematical Aspects*, no. article 101061, 2021Intechopen, 2021.

[46] S. Tang, T. Cai, G. M. Wang, J. G. Liang, X. Li, and J. Yu, "High-efficiency dual-modes vortex beam generator with polarization-dependent transmission and reflection properties," *Scientific Reports*, vol. 8, no. 1, 2018.

[47] H. Zhang, W. Ding, P. Fu et al., "Reducing orbital angular momentum crosstalk of the Bessel–Gaussian beam for underwater optical communications," *Journal of Optics*, vol. 22, no. 6, p. 065702, 2020.

[48] Y. Zhu, Y. Zhang, and G. Yang, "Evolution of orbital angular momentum mode of the autofocusing hypergeometric- Gaussian beams through moderate-to-strong anisotropic non-Kolmogorov turbulence," *Optics Communications*, vol. 405, pp. 66–72, 2017.

[49] Z. Hu, H. Liu, J. Xia et al., "Propagation of orbital angular momentum modes carried by hollow vortex Gaussian beams in anisotropic atmospheric turbulence," *Journal of the Optical Society of America*, vol. 37, no. 9, pp. 1404–1410, 2020.

[50] A. Schutza, "Transmission of quantum information via Laguerre Gaussian modes," *McNair Scholars Journal*, vol. 14, no. 1, p. 8, 2010.

[51] M. Khulbe, M. R. Tripathy, and H. Parthasarathy, "Orbital angular momentum and spin angular momentum new method for radar imaging with wavelet transforms," in *2019 6th International Conference on Signal Processing and Integrated Networks (SPIN)*, pp. 1122–1124, Noida, India, 2019 Mar 7.

[52] Y. Yu, Y. Lian, Q. Hu et al., "Design of PCF supporting 86 OAM modes with high mode quality and low nonlinear coefficient," *Photonics*, vol. 9, no. 4, p. 266, 2022.

[53] M. M. Hassan, M. A. Kabir, M. N. Hossain et al., "Numerical analysis of circular core shaped photonic crystal fiber for orbital angular momentum with efficient transmission," *Applied Physics B*, vol. 126, no. 9, p. 145, 2020.

[54] L. Cheng, W. Hong, and Z.-C. Hao, "Generation of electromagnetic waves with arbitrary orbital angular momentum modes," *Scientific Reports*, vol. 4, p. 4814, 2014.

[55] W. Hang, S. Gao, and B. Huang, "All-fiber second-order optical vortex generation based on strong modulated long-period grating in a four-mode fiber," *Optics Letters*, vol. 42, no. 24, p. 5210, 2017.

[56] F. A. Al-Zahrani and K. Ahmed, "Novel design of dual guided photonic crystal fiber for large capacity transmission in high-speed optics communications with supporting good quality OAM and LP modes," *Alexandria Engineering Journal*, vol. 59, no. 6, pp. 4889–4899, 2020.

[57] M. A. Kabir, M. M. Hassan, M. N. Hossain, B. K. Paul, and K. Ahmed, "Design and performance evaluation of photonic crystal fibers of supporting orbital angular momentum states in optical transmission," *Optics Communications*, vol. 467, article 125731, 2020.

[58] M. Hassan, M. Kabir, M. Hossain, B. Biswas, B. K. Paul, and K. Ahmed, "Photonic crystal fiber for robust orbital angular momentum transmission: design and investigation," vol. 28, Springer Science+Business Media, Springer Nature, 2020.

[59] A. Jurado-Navas, A. Tatarczak, X. Lu, J. J. Olmos, J. M. Garrido-Balsells, and I. T. Monroy, "850-nm hybrid fiber/free-space optical communications using orbital angular momentum modes," *Optics Express*, vol. 23, no. 26, pp. 33721–33732, 2015.

[60] T. Nakayama, Y. Takayama, C. Fujikawa, and K. Kodate, "Reduction of atmospheric turbulence using optical duplicate system in free-space optical communications," *Optical Review*, vol. 28, no. 4, pp. 434–439, 2021.

[61] X. Yan, P.-F. Zhang, C.-Y. Fan, and J.-H. Zhang, "Effect of atmospheric turbulence on orbital angular momentum entangled state," in *Communications in Theoretical Physics*, vol. 74, no. 2, 2022Chinese Physical Society and IOP Publishing, 2022.

[62] M. Charnotskii, "Transverse linear and orbital angular momenta of beam waves and propagation in random media," *Journal of Optics*, vol. 20, no. 2, article 025602, 2018.

[63] H. Yuksel, *OAI conference*, SPIE Optics & Photonics, 2005.

[64] G. Schirripa Spagnolo, L. Cozzella, and F. Leccese, "Underwater optical wireless communications: overview," *Sensors*, vol. 20, no. 8, p. 2261, 2020.

[65] "Free space optics (FSO) with capacity 10 gigabits full duplex-EC system," ecsystem.cz., praguebest.cz, Prague Best s. r.o. Retrieved 14 March 2018.

[66] R. Paschotta, "Hermite–GauB-modes-another," https://www.rp-photonics.com/hermite_gaussian_modes.html.

[67] Y. Yue, Y. Yan, and N. Ahmed, "Mode properties and propagation effects of optical orbital angular momentum (OAM) modes in a ring fiber," *IEEE Photonics Journal*, vol. 4, no. 2, pp. 535–543, 2012.

[68] I. B. Djordjeric and M. Arabaci, "LDPC-coded orbital angular momentum (OAM) modulation for free-space optical communication," *Optics express*, vol. 18, no. 24, pp. 24722–24728, 2010.